ylated at low levels in mock infected cells, whereas no significant changes in phosphorylation level of these kinases were observed after virus infection. These observations suggest that Tyr-705 dephosphorylation of STAT3 in virus-infected cells occurred independent of its upstream kinases. Therefore, total activity of STAT3 may be low in Vero E6 cells. However, it can not be ruled out that the anti-phospho JAK1, JAK2 and Tyk2 antibodies used in the present study are difficult to be recognized in the phosphorylated JAK1, JAK2 and Tyk2 in Vero E6 cells as the datasheet included no description of cross-reactivity with monkey.

3.3. Stimulation of Tyr-705 phosphorylation of STAT3 by cytokines

Previous studies have indicated that at least six cytokines, IL-2, IL-6, IL-10, IL-15, IL-17, and IL-22, can stimulate activation of STAT3 [21–24]. Tyr-705 dephosphorylation of STAT3 in virus-infected cells may be due to a lack of stimulation by these cytokines after 18 h.p.i. Therefore, it is important to identify the cytokines responsible for stimulating Tyr phosphorylation of STAT3 to understand the mechanism of Tyr-705-dephosphorylation of STAT3 in virus-infected cells. To investigate whether fetal calf serum (FCS) in the medium contains stimulators for STAT3 phosphorylation, Vero E6 cells were cultured in DMEM containing 0%, 2% or 5% FCS for 18 h, subjected to subcellular fractionation, and then the proteins were analyzed by Western blotting using anti-phospho-specific antibodies. As shown in Fig. 3A, there were no significant differences in total amount of STAT3 in cultures with various concentrations of FCS in the medium. This result suggests that FCS does not contain components that stimulate Tyr-phosphorylation of STAT3. We next determined cytokines and their receptors produced in Vero E6 cells using a GEArray Q Series Human Interleukin and Receptor Gene Array (SuperArray Bioscience Corporation, Frederick, MD, USA). Expression level of IL-22, which has also been reported as a stimulator of STAT3 [23], was very low, and receptors for IL-22 (IL-22RA1 and RA2) were obtained as strong and weak signals, respectively (data not shown). Therefore, we examined whether IL-22 stimulated Tyr-705 and Ser-727 phosphorylation of STAT3. As shown in Fig. 4A, the level of Tyr-705-phosphorylated STAT3 increased 15 min after treatment with murine IL-22 (200 ng/ml) (Pepro Tech EC, London, UK), whereas phosphorylation of Ser-727 was not enhanced, suggesting that it is difficult for Ser-727 of

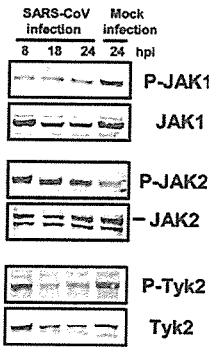

Fig. 2. Phosphorylation levels of upstream kinases of STAT3 in virus-infected cells. Western blotting analyses were performed using anti-phospho JAK1, JAK2, and Tyk2 antibodies.

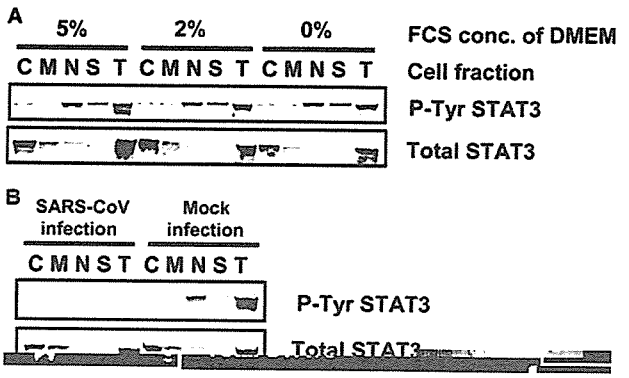

Fig. 3. Subcellular localization of Tyr-phosphorylated STAT3. (A) Vero E6 cells were incubated in DMEM containing 0%, 2% or 5% FCS for 18 h. After subcellular fractionation, Western blotting was performed using anti-phospho STAT3 (Tyr) antibody. (B) C, M, N, S, and T indicate cytosolic, organelle/membrane, nuclear, cytoskeletal, and total cellular fraction, respectively.

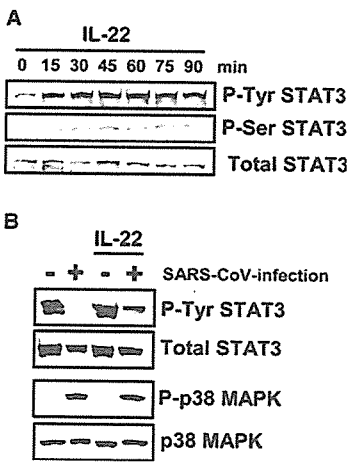

Fig. 4. IL-22 induces Tyr phosphorylation of STAT3. (A) Vero E6 cells were treated with IL-22 from 0 to 90 min. Cellular proteins were sampled every 15 min. Western blotting was performed using anti-phospho STAT3 (Tyr and Ser) antibodies. (B) SARS-CoV-infected Vero E6 cells were treated with IL-22 for 20 min at 18 h.p.i., and then, Western blot analysis was performed using anti-phospho STAT3 (Tyr) and anti-phospho p38 MAPK.

STAT3 to be phosphorylated in Vero E6 cells stimulated by SARS-CoV infection and IL-22. Although the phosphorylation level of p38 MAPK was not changed in SARS-CoV-infected Vero E6 cells by treatment with IL-22 for 20 min at 18 h.p.i., the Tyr-705-phosphorylation of STAT3 increased (Fig. 4B). These results suggest that signaling pathway via IL-22 is not regulated by p38 MAPK in Vero E6 cells.

3.4. Tyr-705-phosphorylated STAT3 in the nucleus

To determine the localization of Tyr-705-phosphorylated STAT3 in Vero E6 cells, subcellular extraction was performed using a Subcellular Proteome Extraction Kit (Calbiochem) and then Western blotting analyses were performed. As described above, the amounts of total and Tyr-705-phosphorylated STAT3 were similar in cells grown in media containing 0%, 2% or 5% FCS. The subcellular localization of STAT3 was not

affected by the concentration of FCS (Fig. 3A). Total STAT3 was located mainly in the cytosol, and also in membranes/organelles and the nuclear fractions. On the other hand, Tyr-705-phosphorylated STAT3 appeared mainly in the nuclear fraction. We next examined whether Tyr-705-phosphorylated STAT3 was not present in the nucleus in SARS-CoV-infected Vero E6 cells at 18 h.p.i. As shown in Fig. 3B, Tyr-705-phosphorylated STAT3 had clearly disappeared from the nuclear fraction in virus-infected cells. This result strongly suggested that STAT3 did not act as a transcriptional enhancer in SARS-CoV-infected Vero E6 cells after 18 h.p.i.

3.5. Phosphorylation of MAPKs in SARS-CoV-infected cells

Our previous report indicated that SARS-CoV-infection to Vero E6 induced phosphorylation of p38 MAPK and its downstream targets, HSP-27, eIF4E and CREB [3]. Phosphorylation of these proteins was prevented by treatment of the cells with the p38 MAPK inhibitor SB20854. MAPKs were reported to induce Ser-727 phosphorylation of STAT3 [25]. To investigate whether other MAPKs, i.e., ERK1/2 (extracellular signal-regulated kinase) and JNK, are also phosphorylated in SARS-CoV-infected Vero E6 cells, the kinetics of phosphorylation of ERK1/2 and JNK were analyzed by Western blotting. Vero E6 cells were infected with SARS-CoV at m.o.i. of 10 and the cell extracts were prepared at various time points after infection. Western blotting analysis demonstrated that levels of phosphorylated ERK1/2 and JNK were increased in SARS-CoV-infected cells (Fig. 5A). Two phosphorylated forms of ERK, ERK1 and ERK2, were detected at 12 h.p.i. and accumulated continuously up to 24 h.p.i. The kinetics of accumulation of phosphorylated ERK1/2 and JNK in the infected cells were similar to that of accumulation of phosphorylated p38 MAPK. We next examined whether the upstream MAPK kinases (MAPKKs) were also phosphorylated in SARS-CoV-infected Vero E6 cells. The kinases of p38, ERK1/2, and JNK are known as MKK3/6, MEK1/2, and MKK4/7, respectively. As shown in Fig. 5, MKK3/6, MEK1/2, and MKK4/7 were phosphorylated in SARS-CoV-infected Vero E6 cells.

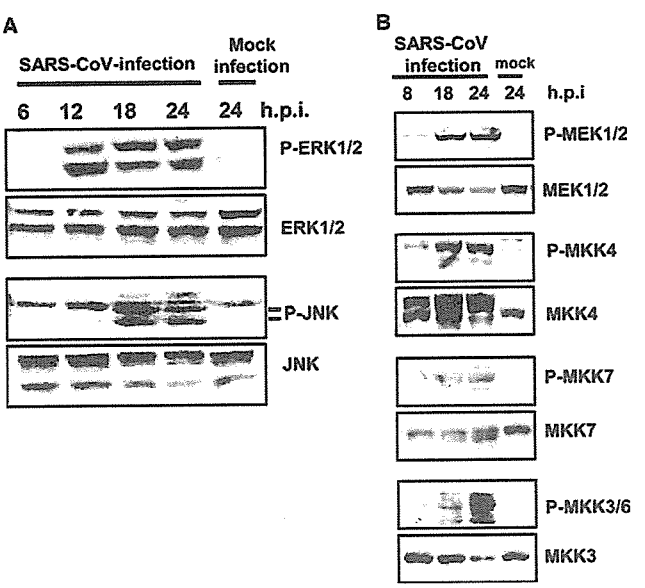

Fig. 5. MAPKs phosphorylation in virus-infected cells. Western blotting analysis of proteins from SARS-CoV-infected Vero E6 cells was performed using anti-phospho ERK1/2, JNK, MEK1/2, MKK4, MKK7, and MKK3/6 antibodies.

3.6. Tyr dephosphorylation of STAT3 by p38 MAPK

To investigate whether Tyr-705 phosphorylation is regulated by activated MAPKs in SARS-CoV-infected Vero E6 cells, the infected cells were treated for 18 h with three MAPK inhibitors: SB203580 (p38 MAPK inhibitor), PD98059 (MEK inhibitor), and SP600125 (JNK inhibitor). Tyr-705- and Ser-727-phosphorylated STAT3 were then analyzed by Western blotting. As shown in Fig. 6A, SB203580 did not affect Ser-727 phosphorylation of STAT3, while SARS-CoV-induced dephosphorylation of STAT3 Tyr-705 was partially inhibited by SB203580. On the other hand, neither PD98059 nor SP600125 affected STAT3 phosphorylation. To confirm whether inhibition of p38 prevents dephosphorylation of STAT3 Tyr-705, virus-infected cells were treated with another p38 inhibitor, SB202190. As shown in Fig. 6B, Tyr-705 dephosphorylation of STAT3 in the infected cells was also partially inhibited by SB202190. These results indicated that activated p38 MAPK in SARS-CoV-infected Vero E6 cells regulates Tyr-705 phosphorylation of STAT3, but not that of Ser-727.

4. Discussion

In the present and previous studies, we reported that the cellular mechanisms by which SARS-CoV caused the activation of physiological intracellular signaling cascades that lead to the phosphorylation and activation of downstream molecules [3,4]. We showed here that SARS-CoV-infection of permissive Vero E6 cells stimulated p38, ERK1/2, and JNK

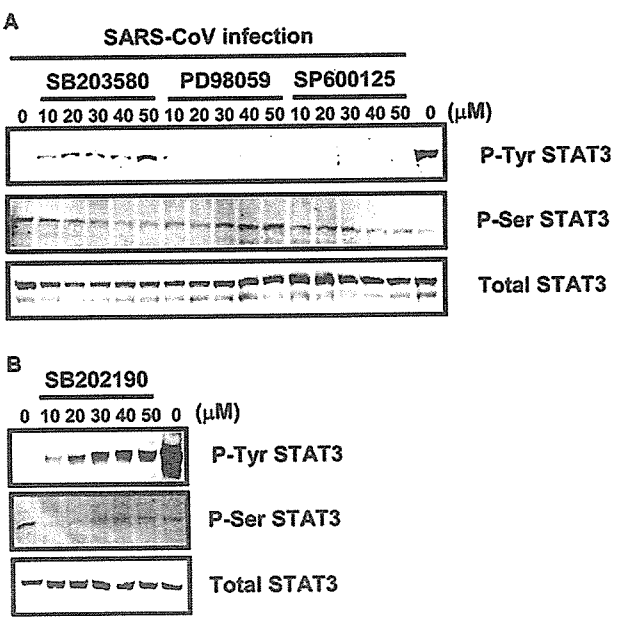

Fig. 6. Effects of treatment of SARS-CoV-infected Vero E6 cells with p38 MAPK inhibitor. (A) Vero E6 cells were infected with SARS-CoV at m.o.i. of 10, and then incubated with SB203580, PD98059, and SP600125 at concentrations from 10 to 50 μM for 17 h. Western blotting analyses were performed to detect Tyr-705- and Ser-727-phosphorylated forms of STAT3. (B) SB202190 was used as a p38 MAPK inhibitor.

signaling pathways. The activation of p38 MAPK induces cytopathic effects in Vero E6 cells, whereas ERK1/2 and JNK had no effect (unpublished data). As MAPKKs for p38, ERK1/2, and JNK were all phosphorylated in virus-infected cells, further studies are needed to identify triggers of the stress-activated response pathway by viral infection. The present study strongly suggested that the p38 MAPK signaling pathway is upstream of Tyr-705 dephosphorylation of STAT3. We also demonstrated that infection with SARS-CoV slightly increased the level of phosphorylation of Ser-727 STAT3. Although the effect of Ser-727 phosphorylation on the function of STAT3 in SARS-CoV-infected cells remains unresolved, a previous study showed that phosphorylation of Ser-727 of STAT3 negatively modulates its tyrosine phosphorylation [26]. Thus, the timing of Tyr-705 dephosphorylation and Ser-727 phosphorylation may be almost the same in SARS-CoV-infected cells. The Ser-727-phosphorylated STAT3-mediated expression of a Bcl-2 family member, Mcl-1, is essential for the survival of cells [27], suggesting that Ser-727-phosphorylated STAT3 has anti-apoptotic activity. However, the mechanism through which serine phosphorylation regulates the transcriptional activities of STAT3 is still unclear. On the other hand, one of the important roles of Tyr-705-phosphorylated STAT3 is binding to regulatory DNA elements that control the expression of target genes [28,29]. Suppression of STAT3 expression by siRNA induces apoptosis in several astrocytoma cell lines, and STAT3 is required for the expression of the anti-apoptotic genes survivin and Bcl-xL in the A172 glioblastoma cell line [30]. In addition, the role of STAT proteins during viral infection has been the subject of several recent studies. The proteasome-dependent degradation of STAT1 is induced by V protein of simian virus 5 [31], while type II human parainfluenza virus V protein targets STAT2, and mumps virus V protein targets both STAT1 and STAT3 [32–34]. In measles virus-infected cells, the V protein forms complexes with STAT1, STAT2, and STAT3, and inhibits both IL-6- and v-Src STAT3-dependent signaling [16]. Thus, a role of V protein as an inhibitor of the STAT3 signaling pathway is advantageous for viral growth. SARS-CoV may also obtain a growth advantage by Tyr-705 dephosphorylation of STAT3.

Our recent study indicated that Akt was also activated in response to SARS-CoV-replication [4]. Although phosphorylation of serine residue 473 on Akt was detected at least 8 h.p.i., threonine residue 308 was not phosphorylated in virus-infected Vero E6 cells. A downstream target of Akt, glycogen synthase kinase 3β (GSK-3β), was slightly phosphorylated, indicating that the level of activation of Akt was very low. The present study showed that IL-22 can induce Tyr-705 phosphorylation of STAT3, but not Ser-727 phosphorylation, similarly to SARS-CoV infection. It may be difficult for Ser-727 of STAT3 to be phosphorylated in Vero E6 cells, similarly to Thr-308 of Akt. Based on these results, we hypothesized that weak activation of Akt cannot prevent apoptosis induced by SARS-CoV infection in Vero E6 cells. In SARS-infected Vero E6 cells, both incomplete activation of Akt and STAT3 dephosphorylation via p38 MAPK activation lead to apoptotic cell death. We assume that these are at least part of the mechanisms of the pathogenesis of SARS-CoV infection.

Acknowledgements: We thank Drs. F. Taguchi (National Institute of Infectious Diseases, Japan) and H. Shima, O. Inanami (Hokkaido University, Japan) for helpful suggestions. We also thank Ms. M. Ogata (National Institute of Infectious Diseases, Japan) for her assistance. This work was supported in part by a grant-in-aid from the Ministry of Health, Labor, and Welfare of Japan and the Japan Health Science Foundation, Tokyo, Japan.

References

[1] Rota, P.A., Oberste, M.S., Monroe, S.S., Nix, W.A., Campagnoli, R., Icenogle, J.P., Penaranda, S., Bankamp, B., Maher, K., Chen, M.H., Tong, S., Tamin, A., Lowe, L., Frace, M., DeRisi, J.L., Chen, Q., Wang, D., Erdman, D.D., Peret, T.C., Burns, C., Ksiazek, T.G., Rollin, P.E., Sanchez, A., Liffick, S., Holloway, B., Limor, J., McCaustland, K., Olsen-Rasmussen, M., Fouchier, R., Gunther, S., Osterhaus, A.D., Drosten, C., Pallansch, M.A., Anderson, L.J. and Bellini, W.J. (2003) Science 300, 1394–1399.
[2] Marra, M.A., Jones, S.J., Astell, C.R., Holt, R.A., Brooks-Wilson, A., Butterfield, Y.S., Khattra, J., Asano, J.K., Barber, S.A., Chan, S.Y., Cloutier, A., Coughlin, S.M., Freeman, D., Girn, N., Griffith, O.L., Leach, S.R., Mayo, M., McDonald, H., Montgomery, S.B., Pandoh, P.K., Petrescu, A.S., Robertson, A.G., Schein, J.E., Siddiqui, A., Smailus, D.E., Stott, J.M., Yang, G.S., Plummer, F., Andonov, A., Artsob, H., Bastien, N., Bernard, K., Booth, T.F., Bowness, D., Czub, M., Drebot, M., Fernando, L., Flick, R., Garbutt, M., Gray, M., Grolla, A., Jones, S., Feldmann, H., Meyers, A., Kabani, A., Li, Y., Normand, S., Stroher, U., Tipples, G.A., Tyler, S., Vogrig, R., Ward, D., Watson, B., Brunham, R.C., Krajden, M., Petric, M., Skowronski, D.M., Upton, C. and Roper, R.L. (2003) Science 300, 1399–1404.
[3] Mizutani, T., Fukushi, S., Saijo, M., Kurane, I. and Morikawa, S. (2004) Biochem. Biophys. Res. Commun. 319, 1228–1234.
[4] Mizutani, T., Fukushi, S., Saijo, M., Kurane, I. and Morikawa, S. (2004) Virology 327, 169–174.
[5] Garrington, T.P. and Johnson, G.L. (1999) Curr. Opin. Cell. Biol. 11, 211–218.
[6] Whitmarsh, A.J. and Davis, R.J. (2003) Nature 403, 255–256.
[7] Chang, L. and Karin, M. (2001) Nature 410, 37–40.
[8] Kyriakis, J.M. and Avruch, J. (2001) Physiol. Rev. 81, 807–869.
[9] Shuai, K., Stark, G.R., Kerr, I.M. and Darnell Jr., J.E. (1993) Science 261, 1744–1746.
[10] Shuai, K., Horvath, C.M., Huang, L.H., Qureshi, S.A., Cowburn, D. and Darnell Jr., J.E. (1994) Cell 76, 821–828.
[11] Shuai, K., Schindler, C., Prezioso, V.R. and Darnell Jr., J.E. (1992) Science 258, 1808–1812.
[12] Schindler, C., Shuai, K., Prezioso, V.R. and Darnell Jr., J.E. (1992) Science 257, 809–813.
[13] Rajan, P. and McKay, R.D. (1998) J. Neurosci. 18, 3620–3629.
[14] Grandis, J.R., Drenning, S.D., Zeng, Q., Watkins, S.C., Melhem, M.F., Endo, S., Johnson, D.E., Huang, L., He, Y. and Kim, J.D. (2000) Proc. Natl. Acad. Sci. USA 97, 4227–4232.
[15] Mora, L.B., Buettner, R., Seigne, J., Diaz, J., Ahmad, N., Garcia, R., Bowman, T., Falcone, R., Fairclough, R., Cantor, A., Muro-Cacho, C., Livingston, S., Karras, J., Pow-Sang, J. and Jove, R. (2002) Cancer Res. 62, 6659–6666.
[16] Palosaari, H., Parisien, J.-P., Rodriguez, J.J., Ulane, C.M. and Horvath, C.M. (2003) J. Virol. 77, 7635–7644.
[17] Thiel, V., Ivanov, K.A., Putics, A., Hertzig, T., Schelle, B., Bayer, S., Weissbrich, B., Snijder, E.J., Rabenau, H., Doerr, H.W., Gorbalenya, A.E. and Ziebuhr, J. (2003) J. Gen. Virol. 84, 2305–2315.
[18] Mizutani, T., Kobayashi, M., Eshita, Y., Shirato, K., Kimura, T., Ako, Y., Miyoshi, H., Takasaki, T., Kurane, T., Kariwa, H., Umemura, T. and Takashima, I. (2003) Insect. Mol. Biol. 12, 491–499.
[19] Garcia, R., Yu, C.-L., Hudnall, A., Catlett, R., Nelson, K.L., Smithgall, T., Fujita, D.J., Ethier, S.P. and Jove, R. (1997) Cell Growth Differ. 8, 1267–1276.
[20] Kerr, I.M., Costa-Pereira, A.P., Lillemeier, B.F. and Strobl, B. (2003) FEBS Lett. 546, 1–5.
[21] Niemand, C., Nimmesgern, A., Haan, S., Fischer, P., Schaper, F., Rossaint, R., Heinrich, P.C. and Muller-Newen, G. (2003) J. Immunol. 170, 3263–3272.
[22] Nielsen, M., Nordahl, M., Svejgaard, A. and Odum, N. (1998) Cytokine 10, 735–738.

[23] Subramaniam, S.V., Cooper, R.S. and Adunyah, S.E. (1999) Biochem. Biophys. Res. Commun. 262, 14–19.
[24] Lejeune, D., Dumoutier, L., Constantinescu, S., Kruijer, W., Schuringa, J.J. and Renauld, J.C. (2002) J. Biol. Chem. 277, 33676–33682.
[25] Haq, R., Halupa, A., Beattie, B.K., Mason, J.M., Zanke, B.W. and Barber, D.L. (2002) J. Biol. Chem. 277, 17359–17366.
[26] Chung, J., Uchida, E., Grammer, T.C. and Blenis, J. (1997) Mol. Cell. Biol. 17, 6508–6516.
[27] Liu, H., Ma, Y., Cole, S.M., Zander, C., Chen, K.H., Karras, J. and Pope, R.M. (2003) Blood 102, 344–352.
[28] Wegenka, U.M., Buschmann, J., Lutticken, C., Heinrich, P.C. and Horn, F. (1993) Mol. Cell. Biol. 13, 276–288.
[29] Yuan, J., Wegenka, U.M., Lutticken, C., Buschmann, J., Decker, T., Schindler, C., Heinrich, P.C. and Horn, F. (1994) Mol. Cell. Biol. 14, 1657–1668.
[30] Konnikova, L., Kotecki, M., Kruger, M.M. and Cochran, B.H. (2003) BMC Cancer 3, 3–23.
[31] Didcock, L., Young, D.F., Goodbourn, S. and Randall, R.E. (1999) J. Virol. 73, 9928–9933.
[32] Parisien, J.-P., Lau, J.F., Rodriguez, J.J., Sullivan, B.M., Moscona, A., Parks, G.D., Lamb, R.A. and Horvath C.M (2001) J. Virol. 283, 230–239.
[33] Nishio, M., Garcin, D., Simonet, V. and Kolakofsky, D. (2002) Virology 300, 92–99.
[34] Ulane, C.M., Rodriguez, J.J., Parisien, J.-P. and Horvath, C.M. (2003) J. Virol. 77, 6385–6393.

International Immunology, Vol. 16, No. 10, pp. 1423–1430
doi:10.1093/intimm/dxh143 Advance Access publication 16 August 2004

A subcutaneously injected UV-inactivated SARS coronavirus vaccine elicits systemic humoral immunity in mice

Naomi Takasuka[1], Hideki Fujii[1], Yoshimasa Takahashi[1], Masataka Kasai[1], Shigeru Morikawa[2], Shigeyuki Itamura[4], Koji Ishii[3], Masahiro Sakaguchi[1], Kazuo Ohnishi[1], Masamichi Ohshima[1], Shu-ichi Hashimoto[1], Takato Odagiri[4], Masato Tashiro[4], Hiroshi Yoshikura[5], Toshitada Takemori[1] and **Yasuko Tsunetsugu-Yokota[1]**

[1]Department of Immunology, [2]First, [3]Second and [4]Third Departments of Virology, [5]National Institute of Infectious Diseases, Toyama 1-23-1, Shinjuku-ku, Tokyo 162-8640, Japan

Keywords: alum, cellular immunity, neutralizing antibody, parenteral administration, vaccination

Abstract

The recent emergence of severe acute respiratory syndrome (SARS) was caused by a novel coronavirus, SARS-CoV. It spread rapidly to many countries and developing a SARS vaccine is now urgently required. In order to study the immunogenicity of UV-inactivated purified SARS-CoV virion as a vaccine candidate, we subcutaneously immunized mice with UV-inactivated SARS-CoV with or without an adjuvant. We chose aluminum hydroxide gel (alum) as an adjuvant, because of its long safety history for human use. We observed that the UV-inactivated SARS-CoV virion elicited a high level of humoral immunity, resulting in the generation of long-term antibody secreting and memory B cells. With the addition of alum to the vaccine formula, serum IgG production was augmented and reached a level similar to that found in hyper-immunized mice, though it was still insufficient to elicit serum IgA antibodies. Notably, the SARS-CoV virion itself was able to induce long-term antibody production even without an adjuvant. Anti-SARS-CoV antibodies elicited in mice recognized both the spike and nucleocapsid proteins of the virus and were able to neutralize the virus. Furthermore, the UV-inactivated virion induced regional lymph node T-cell proliferation and significant levels of cytokine production (IL-2, IL-4, IL-5, IFN-γ and TNF-α) upon restimulation with inactivated SARS-CoV virion *in vitro*. Thus, a whole killed virion could serve as a candidate antigen for a SARS vaccine to elicit both humoral and cellular immunity.

Introduction

A new disease called severe acute respiratory syndrome (SARS) originated in China in late 2002 and spread rapidly to many countries. Upon this outbreak, a global collaboration network was coordinated by WHO. As a result of this unprecedented international effort, a novel type of coronavirus (SARS-CoV) was identified as the etiologic agent of SARS (1,2) in March 2003. The genomic sequence of SARS-CoV was completed and we now know that SARS-CoV has all the features and characteristics of other coronaviruses, but it is quite different from all previously known coronaviruses (groups I~III), representing a new group (group IV) (3,4). It is assumed that SARS-CoV is a mutant coronavirus transmitted from a wild animal that developed the ability to productively infect humans (3,5). The genome of SARS-CoV is a single-stranded plus-sense RNA ~30 kb in length and containing five major open reading frames that encode non-structural replicase polyproteins and structural proteins: the spike (S), envelope (E), membrane (M) and nucleocapsid protein (N), in the same order and of approximately the same sizes as those of other coronaviruses (5).

The reason why SARS-CoV induces severe respiratory distress in some, but not all, infected individuals is still unclear. In patients with SARS and probable SARS cases, virus is detected in sputum, stool and plasma by RT–PCR (1,2). These patients developed serum antibodies against SARS-CoV and high antibody titers against N protein were maintained for more than 5 months after infection (6). Because of their generally poor pathogenicity and difficulty of propagation

Correspondence to: Y. Tsunetsugu-Yokota; E-mail: yyokota@nih.go.jp

Transmitting editor: K. Sugamura

Received 6 May 2004, *accepted* 15 July 2004

in vitro, there have been few studies regarding immunity to human coronaviruses OC43 and 229E. In the veterinary field, however, coronaviruses have been known for many years to cause a variety of lung, liver and gut diseases in animals. As we learned from these animal models, both humoral and cellular immune responses may contribute to protection against coronavirus diseases, including SARS [for review see (7)].

The clinical manifestation of SARS is hardly distinct from other common respiratory viral infections including influenza. Because an influenza epidemic may occur simultaneously with the re-emergence of SARS, it is urgently required that we develop effective SARS vaccines as well as sensitive diagnostic tests specific for SARS. Recently, the angiotensin-converting enzyme 2 (ACE2) was identified as a cellular receptor for SARS-CoV (8). The first step in viral infection is presumably the binding of S protein to its receptor, ACE2. In the murine MHV model, S proteins are known to contain important virus-neutralizing epitopes that elicit neutralizing antibodies in mice (9,10). Therefore, the S protein would be the first candidate coronavirus protein for induction of immunity. However, the S, M and N proteins are also known to contribute to generating the host immune response (11,12).

Following an established vaccine protocol is one of the best ways to shorten the time and cost of new vaccine development. Most of the currently available vaccines for humans are inactivated and applied cutaneously, except oral polio vaccine, and adjuvant usage is mostly limited to aluminum hydroxide gel (alum). In order to know the immunogenicity of inactivated SARS-CoV as a vaccine candidate, we immunized mice with UV-inactivated SARS-CoV either with or without alum. We report here the evaluation of humoral and cellular immunity elicited by UV-inactivated SARS-CoV administered subcutaneously.

Methods

Preparation of UV-inactivated purified SARS-CoV

SARS-CoV (HKU39849) was kindly supplied by Dr J.S.M. Peiris, Department of Microbiology, The University of Hong Kong. The virus was amplified in Vero E6 cells and purified by sucrose density gradient centrifugation. Concentrated virus was then exposed to UV light (4.75 J/cm^2) in order to inactivate the virus. We confirmed that the virus completely lost its infectivity by this method.

Immunization of mice

Female BALB/c mice were purchased from Nippon SLC Inc. (Shizuoka, Japan) and were housed under specific pathogen-free conditions. All experimental procedures were carried out under NIID-recommended guidelines. Mice were subcutaneously injected via their back or right and left hind leg footpads with 10 μg of UV-inactivated purified SARS-CoV with or without 2 mg of alum, and boosted by the same procedure 7 weeks after priming.

Detection of immunoglobulins in the serum samples

Blood was obtained from the tail vein and allowed to clot overnight at 4°C. Sera were then collected by centrifugation. For ELISA, microtiter plates (Dynatech, Chantily, VA) were coated overnight at 4°C with SARS-CoV-infected or mock-infected Vero E6 cell lysates, which had been treated with 1% NP40 followed by UV-inactivation. To detect S or N protein, the plates were coated with 1% NP40 lysates of chick embryo fibroblasts that had been infected with S or N protein-expressing DIs (attenuated vaccinia virus) (13). The plates were blocked with 1% OVA in PBS–Tween (0.05%) and then incubated with the sera serially diluted at 1:25–1:10^5 for 1 h at room temperature. Plates were incubated with either peroxidase-conjugated anti-mouse IgG (1:2000, Zymed, San Francisco, CA), IgM or IgA (1:2000, Southern Biotechnology, Birmingham, AL) antibody. For detection of IgG subclasses, either peroxidase-conjugated anti-mouse IgG_1, IgG_{2a}, IgG_{2b} (1:2000, Zymed) or IgG_3 (1:2000, Southern Biotechnology) was used. Plates were washed three times with PBS–Tween at each step. Antibodies were detected by *O*-phenylenediamine (Zymed), and the absorbance of each well was read at 490 nm using a model 680 microplate reader (Bio-Rad, Hercules, CA). As a standard for IgG detection, serum was obtained from a hyper-immunized mouse; the OD490nm value of 100 U/ml standard was ~3 in all assays. SARS-CoV-specific IgG titer was calculated as follows: SARS-specific IgG titer (U/ml) = (the unit value obtained at wells coated with virus-infected cell lysates) – (the unit value obtained at wells coated with non-infected cell lysates).

ELISPOT assay for antibody-secreting cells (ASCs)

Recombinant N protein (amino acids 1–49 and 340–390) of SARS-CoV (Biodesign, Saco, ME) was diluted to 10 μg/ml in PBS, and then added at 100 μl per well to plates supported by a nitrocellulose filter (Millipore, Bedford, MA). After overnight incubation at 4°C, the plates were washed with PBS three times and then blocked at 4°C overnight with 1% OVA in PBS–Tween (0.05%). After erythrocyte lysis, single cell suspensions from BMs were suspended in RPMI supplemented with 10% FCS, 5 × 10^{-5} M 2ME, 2 mM L-glutamine, 100 U/ml penicillin and 100 μg/ml streptomycin, and then applied to the plates at a concentration of 3 × 10^5 cells per well. After 24 h cultivation, the plates were recovered and stained with alkaline phosphatase-conjugated anti-mouse IgG_1 antibody (Southern Biotechnologies). Alkaline phosphatase activity was visualized using 3-amino-ethyl carbozole and napthol AS-MX phosphate/fast blue BB (Sigma). The frequency of plasma cells specific for N protein was determined from the N protein-coated plates after background on the uncoated plates was subtracted.

Coronavirus neutralizing assay

Serum was inactivated by incubation at 56°C for 30 min. The known tissue culture infectious dose (TCID) of SARS-CoV was incubated for 1 h in the presence or absence of serum antibodies serially diluted 5-fold, and then added to Vero E6 cell culture grown confluently in a 96-well microtiter plate. After 48 h, cells were fixed with 10% formaldehyde and stained with crystal violet to visualize the cytopathic effect induced by the virus (14). Neutralization antibody titers were expressed as the minimum dilution number of serum that inhibited the cytopathic effect.

Western blotting

Purified SARS-CoV virion (0.5 μg) was fractionated on SDS–PAGE under reduced conditions. Proteins were transferred to PVDF membrane (Genetics, Tokyo, Japan) and reacted with the diluted sera (1:1000) that had been obtained from mice inoculated with UV-irradiated SARS-CoV. After washing, the membrane was reacted with HRP-conjugated $F(ab')_2$ fragment anti-mouse IgG (H+L) (1:20 000 Jackson Immuno Research, West Grove, PA), followed by visualization of the bands on X-ray film (Kodak, Rochester, NY) using chemiluminescent regents (Amasham Biosciences, Piscataway, NJ).

Regional T cell response

Popliteal and inguinal lymph nodes and spleens were harvested from mice 1 week after the boost vaccination. After the preparation of a single cell suspension, T cells were purified by depletion of $B220^+$, $Gr1^+$, $CD11b^+$, IgD^+ and IgM^+ cells using a magnetic cell sort system (MACS: Miltenyi Biotec, Bergisch Gladbach, Germany). To prepare antigen-presenting cells (APC), normal BALB/c mouse splenocytes were depleted of $CD3^+$ T cells by MACS and irradiated at 2000 cGy.

Purified T cells taken from lymph nodes (1×10^5 cells/well) were cultured with irradiated APC (5×10^5 cells/well) in the presence or absence of UV-irradiated purified SARS-CoV virion (1 or 10 μg/ml). Four days after the cultivation, the level of cytokine concentration in the culture supernatant was measured by flow cytometry using a mouse Th1/Th2 cytokine cytometric bead array kit (Becton Dickinson, San Jose, CA). T-cell proliferation was monitored by the incorporation of $[^3H]$thymidine (18.5 kBq/well, ICN Biomedicals, Costa Mesa, CA) added 8 h prior to cell harvest. The cells were harvested on a 96-well microplate bonded with a GF/B filter (Packard Instruments, Meriden, CT). Incorporated radioactivity was counted by a microplate scintillation counter (Packard Instruments).

Results

Inoculation with UV-inactivated SARS-CoV results in an antigen-specific IgG_1 response, probably by generating long-term ASCs as well as memory cells

To examine the level of anti-SARS-CoV response in mice after inoculation with vaccine candidates, three mice in each group were subcutaneously inoculated with 10 μg of UV-inactivated purified SARS-CoV with (Virion/Alum) or without alum (Virion), or inoculated with alum alone (Alum) or left untreated (None) as a control (Fig. 1). One month after inoculation, vaccinated mice elicited the anti-SARS CoV IgG antibody in sera at high levels. As expected, the alum adjuvant enhanced the level of IgG antibody response, >10-fold higher than the level without adjuvant (Fig. 1C compared with B). When mice were boosted at 7 weeks, the level of IgG antibody in both groups of mice was further increased ~10-fold above the primary response (Fig. 1B and C). Notably, the level of serum antibodies induced by a single injection of virion, even in the absence of the alum adjuvant, was maintained at least more than 6 months (Fig. 1D). These results suggest that long-term ASCs can be established by a single shot of UV-inactivated virion administration.

Upon restimulation with antigen, memory B cells rapidly differentiate into ASCs and migrate into the bone marrow to establish a long-term ASC pool (15,16). To enumerate the number of plasma cells specific for SARS-CoV, we performed an ELISPOT assay using recombinant N proteins, amino acid numbers 1–49 (N1–49) and 340–390 (N340–390) as coating antigens. Consistent with the serum anti-SARS CoV IgG level, SARS-specific IgG_1 plasma cells were maintained in the bone marrow at day 10 after boost immunization with virion/alum

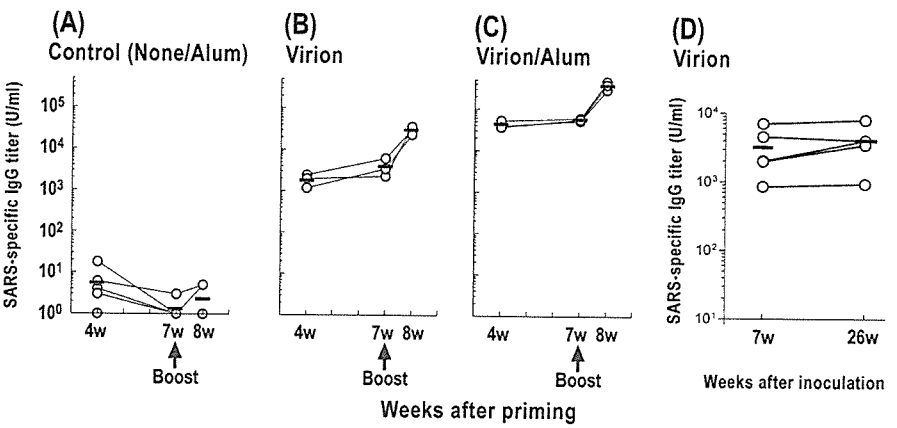

Fig. 1. The level of SARS-specific IgG in subcutaneously vaccinated mice. Mice were subcutaneously primed with 10 μg of UV-inactivated SARS-CoV virion (B), or virion with 2 mg of alum (C), or alum alone or none (A) and boosted with the same dose in their footpads at 7 weeks after priming. Serum was collected at the indicated time point and subjected to ELISA to detect SARS-specific IgG using SARS-CoV-infected Vero cell lysates as a coating antigen. Circles and bars represent the amount of IgG antibody in the serum of each mouse and the mean, respectively. The amount of IgG was arbitrarily calculated based on the concentration of hyper-immune sera. A representative result of two independent experiments is shown. (D) Mice were vaccinated with 10 μg of UV-inactivated SARS-CoV virion subcutaneously into their backs. Serum was collected from individual mice at the indicated time point and subjected to ELISA to detect SARS-specific IgG.

(Fig. 2). In contrast, the number of spots from control mice was below the detection limit (i.e. <1 ASC/9 × 10^5 cells).

UV-inactivated SARS-CoV induces IgG_1 antibody with neutralizing activity

We determined the subclass of serum anti-SARS-CoV IgG antibodies in the boosted mice using anti-mouse IgG_1, IgG_{2a}, IgG_{2b} or IgG_3 second antibody by ELISA (Fig. 3). Interestingly, the level of anti-SARS-CoV IgG_{2a} in mice immunized with virion/alum was comparable to that in mice immunized with virion alone, whereas the level of anti-SARS-CoV IgG_1 was higher in mice with virion/alum than the mice with virion alone. In contrast, the levels of IgG_{2b} and IgG_3 antibodies were fairly low in both groups. Therefore, our results indicated that vaccination with a combination of inactivated virion and alum induced a predominantly Th2-type immune response.

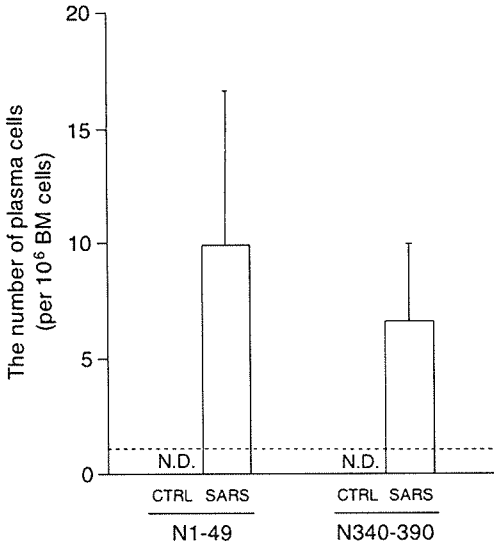

Fig. 2. The number of SARS-specific IgG_1 plasma cells in BM. Mice were primed and boosted by subcutaneous injection into their back with 10 μg of UV-inactivated SARS-CoV virion with 2 mg of alum (VA). BMs were collected at 10 days after boost and subjected to ELISPOT to detect SARS-specific IgG_1 plasma cells. Bars represent the number of plasma cells specific to N1–49 and N340–390 antigen in SARS-vaccinated and control mice, respectively. Data are means of triplicate cultures. The number of spots from control mice was below the detection limit (i.e. <1 ASC/9 × 10^5 cells: dashed line). A representative result of two independent experiments is shown. N.D.: not detected.

We also measured serum immunoglobulins other than IgG in the early and late phases of immunization. To avoid high IgG concentrations interfering with the detection of IgM and IgA antibodies, the serum IgG was absorbed with protein G-conjugated beads (>98%). The levels of anti-SARS-CoV IgM antibodies in the IgG-depleted sera, which were obtained 4 weeks after priming, were below our detection limit. Likewise, anti-SARS-CoV IgA antibody in the IgG-depleted sera, which were obtained 1 week after booster, was not detectable (data not shown).

Whether or not immune sera possess a neutralizing activity against SARS-CoV is a crucial aspect of vaccination. We estimated the neutralizing activity of sera obtained 1 week after boost inoculation (Table 1). We observed that neutralizing activity against SARS-CoV was detected at a high level in sera of mice inoculated with virion/alum or virion alone. Taken together, these results indicate that subcutaneous vaccination with UV-inactivated SARS-CoV virion is able to elicit a sufficient amount of IgG antibodies with neutralizing activity.

UV-inactivated SARS-CoV induces serum IgG antibody specific for S and N proteins

Using the immune sera of mice boosted with virion/alum 1 week before, we analyzed the specificity of serum IgG by western blot analysis (see Methods). As shown in Fig. 4(A), the robust signal detected at 50 kDa corresponds to the N protein of SARS-CoV, as predicted by its genome size (3,4). A band near 200 kDa appears to correspond to S protein, analogous with the S protein of other human coronaviruses, HCV-229E

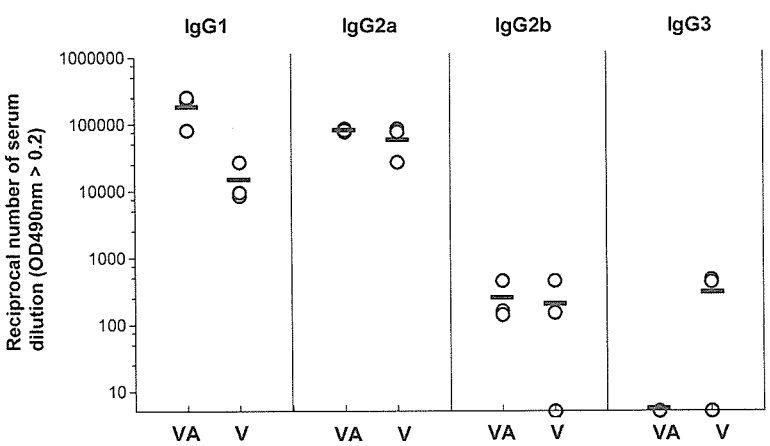

Fig. 3. IgG subclass of immunized serum. Mice were subcutaneously primed and boosted by injection in their footpads with 10 μg of UV-inactivated SARS-CoV virion (V), or virion with 2 mg of alum (VA). Serum was collected from individual mice at 1 week after boost and subjected to ELISA to detect SARS-specific IgG_1, IgG_{2a}, IgG_{2b} and IgG_3 titer. The Y value is the reciprocal serum dilution number where the OD490nm ≥ 0.2 in each ELISA. Circles and bars represent the titer for each mouse and the mean, respectively; results are representative of two separate experiments.

and HCV-OC43, which are known to be heavily glycosylated and detected at 186 kDa and 190 kDa, respectively (17). Our result is consistent with the data reported recently by Xiao *et al.* who expressed the full-length S glycoprotein of SARS-CoV Tor2 strain in 293 cells and showed that the protein ran ~180–200 kDa in SDS gels (18). The origins of the 120 kDa and the faint 37 kDa bands were unknown. However, similar bands were also detected on a fluorogram by using anti-N mAbs (Ohnishi, K., Sakaguchi, M., Takasuka, N. *et al.*, unpublished data), suggesting that it is related to N protein. The specificity of IgG in the immune sera was also determined by ELISA plates coated with lysates of cells infected with either S- or N-expressing recombinant vaccinia viruses (Fig. 4B). The results indicated that anti-S as well as anti-N protein IgG antibodies were elicited by virion/alum vaccination.

Table I. Neutralizing activity in serum after vaccination

		Reciprocal endpoint titer	
		Experiment 1	Experiment 2
None/alum		<5*	<5*
Virion	mouse 1	250	250
	2	1250	250
	3	1250	250
Virion/alum	1	250	1250
	2	1250	1250
	3	1250	1250

*All six mice examined did not have detectable neutralizing activity. Sera were obtained from mice 1 week after boost vaccination and subjected to SARS-CoV neutralizing activity assay as described in Methods. The titer is a reciprocal number of minimum serum dilution that inhibits the cytopathic effect.

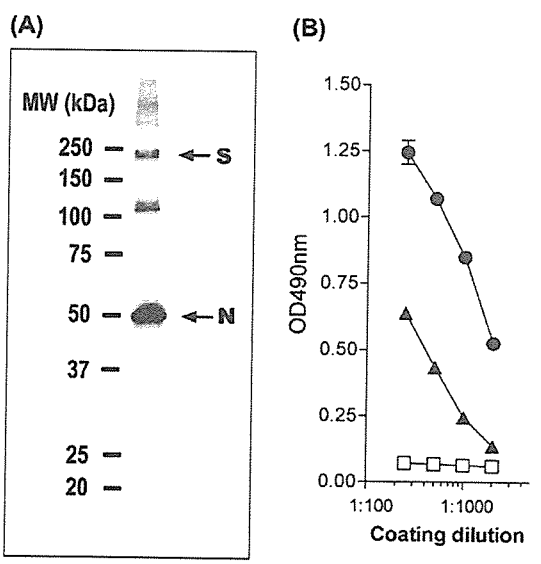

Fig. 4. Specificity of the serum antibodies. (A) Purified UV-inactivated SARS-CoV virion (0.5 μg) was fractionated by SDS–PAGE and subjected to western blotting. Diluted pooled sera (1:1000) from mice primed and boosted with virion/alum were exploited to detect virus proteins. Upper and lower arrows indicate the predicted band of S (spike protein) and N (nucleocapside protein) of SARS-CoV, respectively. The size of molecular weight markers (kDa) is shown on the left. (B) S protein- or N protein-specific ELISA. ELISA plates were coated at the indicated dilution with 1% NP40 lysates of chick embryo fibroblasts that had been infected with S protein-expressing vaccinia virus (circle), N protein-expressing vaccinia virus (triangle) or uninfected (mock; square). Diluted serum (1:1000) from mice prime and boost immunized with virion/alum, was exploited for detection of virus proteins.

UV-inactivated SARS-CoV whole virion induces T-cell response

To examine whether or not subcutaneously vaccinated mice gained an induced T-cell response against SARS-CoV, mice were immunized either with virion/alum, virion, or alum only via the footpad. T cells of these mice were enriched from the spleen and regional lymph nodes 1 week after a booster immunization and cultured with irradiated APCs in the presence or absence of UV-inactivated SARS-CoV virion at 1 or 10 μg/ml. As shown in Fig. 5(A), regional lymph node T cells proliferated *in vitro* in response to UV-inactivated virion in virion/alum-immunized mice and, to a lesser extent, in virion-immunized mice. Because mice inoculated with virion/alum showed a high basal level of proliferation of lymph node T cells in the absence of antigen, there is not much difference in the net proliferative response of these cells between the virion/alum group and the virion only group. On the other hand, in splenic T cells, a low level of proliferation was observed only in the virion/alum group of mice. The level of proliferation of these T cells, however, was virion-dose independent. Therefore, our results suggest that the subcutaneous injection of inactivated virion, even without alum, does induce T cell activation to some extent in the draining lymph node, a result which hardly occurs systemically.

We also measured the level of cytokine production in the supernatant of lymph node T cells stimulated with inactivated virion *in vitro* for 4 days. We found that the inactivated virion induced the production of all the cytokines (IL-2, IL-4, IL-5, IFN-γ and TNF-α) in T cells of virion/alum-immunized mice, in a dose-dependent manner (Fig. 5B). Likewise, T cells of virion-immunized mice produced low, yet significant, levels of these cytokines in a dose-dependent manner, except IL-5. In contrast, lymph node T cells from normal mice did not produce any cytokines at all in response to virion, suggesting that the virion itself does not possess innate stimulating activity as bacterial products [such as lipopolysaccharide (LPS) and purified protein derivative of mycobacterium tuberculosis (PPD)] do. Taken together, these results suggest that subcutaneous vaccination with UV-inactivated SARS-CoV is able to activate $CD4^+$ T cells in regional lymph nodes, where T cells produce several immunoregulatory cytokines, including IFN-γ.

Discussion

The present results demonstrated that even a single subcutaneous administration of UV-irradiated virion without alum adjuvant induced a high level of systemic anti-SARS-CoV antibody response in mice, probably followed by the generation of long-term antibody-secreting cells and memory cells in the bone marrow. Considering that polyvalent particulate

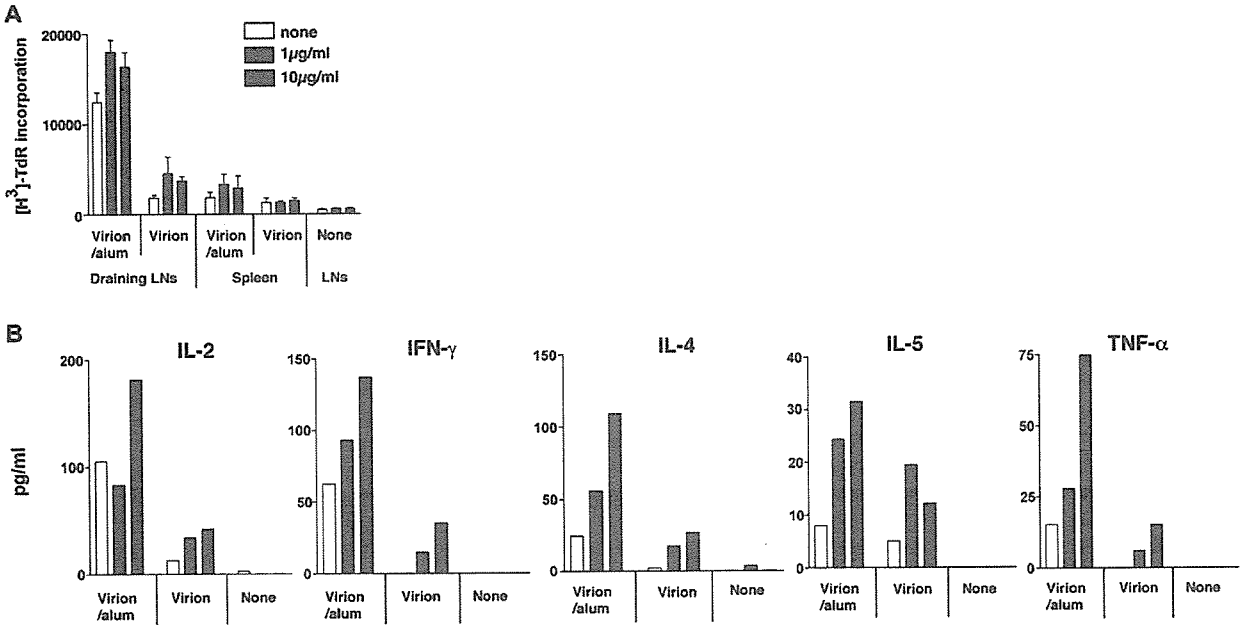

Fig. 5. *In vitro* responses of SARS-CoV-specific T cells taken from mice vaccinated with inactivated SARS-CoV. Mice were subcutaneously primed with 10 μg of UV-inactivated SARS-CoV virion, or virion with 2 mg of alum, or none, and then boosted with the same dose in their footpads at 7 weeks after priming. Draining lymph nodes and spleens were isolated at 1 week after boost and stimulated with T-cell depleted splenocytes that had been pulsed with the indicated concentration of UV-inactivated SARS-CoV virion. These cells were cultured for 2–4 days and [^{3}H]thymidine was added 8 h prior to the harvest. The peak response on day 4 after cultivation is shown in (A). (B) Culture supernatant was collected at day 2–4 post cultivation and the level of IL-2, IFN-γ, IL-4, IL-5 and TNF-α was determined by CBA kit. The maximum cytokine production at day 4 is shown. Results are representative of two separate experiments.

structures such as hepatitis B virus surface antigen-based, HIV-1 Gag-based and Ty virus-like particles have been shown to elicit humoral as well as cellular immune responses (19), these particulates probably have comparable dimensions and structures to the pathogens that are targeted for uptake by APCs to facilitate the induction of potent immune responses. The antibodies elicited in mice vaccinated by the current protocol with or without adjuvant recognized both the S and N proteins of SARS-CoV and were able to neutralize the infection of virus to Vero E6 cells. However, serum anti-SARS-CoV IgA antibody was not detectable, probably owing to the route of vaccination. In addition, the present vaccination protocol caused T cell response at the regional lymph nodes, although it did not allow for the induction of a sufficient cellular immune response systemically.

We show here the potentiality of subcutaneous injection of inactivated virion with alum, which is utilized for most of current human vaccinations. Alum has been used as an adjuvant for vaccines such as diphtheria, pertussis and tetanus, and these vaccines have a long safety record for human use (20). We observed that the addition of alum to the vaccine formula resulted in a large augmentation of serum IgG_1 production, but not IgG_{2a} production. The level of IgG_1 in alum-vaccinated mice reached a level similar to that found in hyper-immunized mice, which were subcutaneously injected with 5 μg of inactivated virion emulsified with a complete Freund adjuvant, followed by consecutive three-times intravenous boosters with 2 μg of virion. Alum is known to selectively stimulate an IgG_1 dominant, type 2 immune response [reviewed in (21)]. Activation of complement by alum could contribute to the type 2-biased immune response partly via an inhibition of IL-12 production. Interestingly, a quite recent report demonstrated that an alum-induced $Gr1^+$ myeloid cell population produced IL-4 and activated B-cells (22).

There are various diseases associated with animal coronavirus infection. The clinical manifestations of the disease and the correlates of protection with immunity have been studied extensively in these animal coronavirus infections [reviewed in (7)]. Although antibodies and T cells may play a role in exacerbating the pathology in some animal coronavirus infections (23,24), both humoral and cellular immune responses are known to contribute to protection against coronavirus infection. In murine hepatitis virus, a Group 2 coronavirus, the mortality of susceptible mice was partially prevented by the transfer of immune serum containing neutralizing antibody prior to challenge (25). Recently, Zhi-yong *et al.* reported in the murine acute infection model that the neutralizing antibody elicited by vaccination of DNA encoding S was protective, but cellular components of vaccinated mice were not required for the inhibition of viral replication (26). Because a twice parenteral administration of inactivated virion with alum induced a high level of antibodies that are able to neutralize SARS-CoV, this vaccination protocol may have a certain effect on the protection of humans from SARS-CoV infection.

We observed that two successive inoculations with inactivated virus at 7 week intervals generated SARS-CoV-specific

T cells. These cells were restimulated with the irradiated virus *in vitro*, but their response was low in terms of the level of proliferation and production of INF-γ and IL-2. However, irrespective of vaccination protocols with or without alum adjuvant, virus-primed T cells of vaccinated animals were capable of producing IL-4 at high levels upon *in vitro* stimulation, comparable to other reports for a variety of vaccination studies (27,28). This outlook seems compatible with the idea that the present vaccine protocol may tend to select T-cell subsets with Th2 phenotype. However, it remains to be elucidated whether such T cells may exhibit serological memory phenotype and persist in the immune system after vaccination as long as memory B cells, which may persist more than 180 days post vaccination. In addition, further analysis is needed to clarify whether T cell response is a crucial factor for long-term protection against SARS-CoV infections.

Efforts to develop a SARS-CoV vaccine have been carried out by many profitable or non-profitable organizations in various ways. For example, it has recently been reported that the combination of adenovirus vector expressing SARS-S, -M or -N protein elicited a neutralizing capacity in serum and N-specific T-cell response in rhesus macaques (29). However, it is still uncertain whether or not the immunity against only these components of SARS-CoV is sufficient for virus protection. SARS-CoV tends to cause replication errors, which may allow the virus to escape the host-immune response and result in a seasonal outbreak. From this point of view, it resembles influenza virus. In influenza virus, inactivated HA vaccine showed incomplete protection but had a certain efficacy and safety record for a long period of time. Indeed, this approach has been used in the veterinary field, such as with the bovine coronavirus (30) and canine coronavirus (31). These advantages make a whole killed virion a prime candidate for a SARS vaccine, even if it may not have the best protective ability.

Unfortunately, no information is available so far on the immune correlates of protection against human coronaviruses, including SARS-CoV. In consideration that SARS-CoV transmission occurs by direct contact with droplets or by the fecal oral route, mucosal secretary IgA in both the lower respiratory tract and digestive tract seem to be crucially important. Failure to induce IgA-type antibodies in a current systemic vaccination method should be improved. Notably, IgA antibodies were detectable in the sera and bronchoalveolar lavage fluid obtained from mice hyper-immunized with UV-irradiated virus (data not shown). Therefore, if a non-toxic and more potent adjuvant becomes available for human use, the subcutaneous injection of inactivated virion would become an effective vaccination method to reduce the number of susceptible people.

In the future, it will be necessary to determine whether or not the inactivated whole virion vaccine possesses protective ability against SARS-CoV infection by the use of adequate animal models. Furthermore, whether the alum addition augmented the protection and the effective period of SARS-CoV virion vaccination should be addressed, because currently used inactivated influenza virus whole virion vaccine is significantly effective without any adjuvant. Meanwhile, we also need to develop a potent adjuvant for induction of a much stronger mucosal immunity, in addition to evaluating available methods of virion inactivation.

Acknowledgements

We thank Ms R. Ishida, Ms Y. Kaburagi and Mr Y. Kimishima for their excellent technical help. This work was supported by a grant from the Ministry of Public Health and Labor of Japan.

Abbreviations

ACE2	angiotensin-converting enzyme 2
ASC	antibody-secreting cell
E	envelope
M	membrane
N	nucleocapsid protein
SARS	severe acute respiratory syndrome
SARS-CoV	SARS-associated coronavirus
S	spike protein

References

1 Drosten, C., Gunther, S., Preiser, W. *et al.* 2003. Identification of a novel coronavirus in patients with severe acute respiratory syndrome. *N. Engl. J. Med.* 348:1967.
2 Ksiazek, T. G., Erdman, D., Goldsmith, C. S. *et al.* 2003. A novel coronavirus associated with severe acute respiratory syndrome. *N. Engl. J. Med.* 348:1953.
3 Marra, M. A., Jones, S. J., Astell, C. R. *et al.* 2003. The genome sequence of the SARS-associated coronavirus. *Science* 300:1399.
4 Rota, P. A., Oberste, M. S., Monroe, S. S. *et al.* 2003. Characterization of a novel coronavirus associated with severe acute respiratory syndrome. *Science* 300:1394.
5 Holmes, K. V. and Enjuanes, L. 2003. Virology. The SARS coronavirus: a postgenomic era. *Science* 300:1377.
6 Liu, X., Shi, Y., Li, P., Li, L., Yi, Y., Ma, Q. and Cao, C. 2004. Profile of antibodies to the nucleocapsid protein of the severe acute respiratory syndrome (SARS)-associated coronavirus in probable SARS patients. *Clin. Diagn. Lab. Immunol.* 11:227.
7 De Groot, A. S. 2003. How the SARS vaccine effort can learn from HIV—speeding towards the future, learning from the past. *Vaccine* 21:4095.
8 Li, W., Moore, M. J., Vasilieva, N. *et al.* 2003. Angiotensin-converting enzyme 2 is a functional receptor for the SARS coronavirus. *Nature* 426:450.
9 Collins, R. A., Knobler, R. L., Powell, H. and Buchmeier, M. J. 1982. Monoclonal antibodies to murine hepatitis virus-4 (strain JHM) define the viral glycoprotein responsible for attachment and cell–cell fusion. *Virology* 119:358.
10 Fleming, J. O., Stohlman, S. A., Harmon, R. C., Lai, M. M., Frelinger, J. A. and Weiner, L. P.1983. Antigenic relationship of murine coronaviruses: analysis using monoclonal antibodies to JHM (MHV-4) virus. *Virology* 131:296.
11 Jackwood, M. W. and Hilt, D. A. 1995. Production and immunogenicity of multiple antigenic peptide (MAP) constructs derived from the S1 glycoprotein of infectious bronchitis virus (IBV). *Adv. Exp. Med. Biol.* 380:213.
12 Anton, I. M., Gonzalez, S., Bullido, M. J., Corsin, M., Risco, C., Langeveld, J. P. and Enjuanes, L. 1996. Cooperation between transmissible gastroenteritis coronavirus (TGEV) structural proteins in the *in vitro* induction of virus-specific antibodies. *Virus Res.* 46:111.
13 Ishii, K., Ueda, Y., Matsuo, K. *et al.* 2002. Structural analysis of vaccinia virus DIs strain: application as a new replication-deficient viral vector. *Virology* 302:433.
14 Storch, G. A. 2001. Diagnostic virology. In Knipe, D. M., Howley, P. M., ed., *Fields Virology*, 4th edn. Lippincott Williams & Wilkins, Philadelphia, PA. pp. 493–531.
15 Benner, R., Hijmans, W. and Haaijman, J. J. 1981. The bone marrow: the major source of serum immunoglobulins, but still a neglected site of antibody formation. *Clin. Exp. Immunol.* 46:1.
16 Slifka, M. K., Matloubian, M. and Ahmed, R. 1995. Bone marrow is a major site of long-term antibody production after acute viral infection. *J. Virol.* 69:1895.
17 Schmidt, O. W. and Kenny, G. E. 1982. Polypeptides and functions of antigens from human coronaviruses 229E and OC43. *Infect. Immun.* 35:515.

18 Xiao, X., Chakraborti, S., Dimitrov, A. S., Gramatikoff, K. and Dimitrov, D. S. 2003. The SARS-CoV S glycoprotein: expression and functional characterization. *Biochem. Biophys. Res. Commun.* 312:1159.
19 Singh, M. and O'Hagan, D. 1999. Advances in vaccine adjuvants. *Nat. Biotechnol.* 17:1075.
20 Clements, C. J. and Griffiths, E. 2002. The global impact of vaccines containing aluminium adjuvants. *Vaccine* 20 (Suppl. 3): S24.
21 HogenEsch, H. 2002. Mechanisms of stimulation of the immune response by aluminum adjuvants. *Vaccine* 20 (Suppl. 3): S34.
22 Jordan, M. B., Mills, D. M., Kappler, J., Marrack, P. and Cambier, J. C. 2004. Promotion of B cell immune responses via an alum-induced myeloid cell population. *Science* 304:1808.
23 Weiss, R. C. and Scott, F. W. 1981. Antibody-mediated enhancement of disease in feline infectious peritonitis: comparisons with dengue hemorrhagic fever. *Comp. Immunol. Microbiol. Infect. Dis.* 4:175.
24 Wu, G. F., Dandekar, A. A., Pewe, L. and Perlman, S. 2001. The role of CD4 and CD8 T cells in MHV-JHM-induced demyelination. *Adv. Exp. Med. Biol.* 494:341.
25 Pope, M., Chung, S. W., Mosmann, T., Leibowitz, J. L., Gorczynski, R. M. and Levy, G. A. 1996. Resistance of naive mice to murine hepatitis virus strain 3 requires development of a Th1, but not a Th2, response, whereas pre-existing antibody partially protects against primary infection. *J. Immunol.* 156:3342.
26 Yang, Z. Y., Kong, W. P., Huang, Y., Roberts, A., Murphy, B. R., Subbarao, K. and Nabel, G. J. 2004. A DNA vaccine induces SARS coronavirus neutralization and protective immunity in mice. *Nature* 428:561.
27 Mazumdar, T., Anam, K. and Ali N. 2004. A mixed Th1/Th2 response elicited by a liposomal formation of *Leishmania* vaccine instructs Th1 responses and resistance to *Leishmania donovani* in susceptible BALB/c mice. *Vaccine* 22:1162.
28 Nicollier-Jamot, B., Ogier, A., Piroth, L., Pothier, P. and Kohli, E. 2004. Recombinant virus-like particles of a norovirus (genogroup II strain) administered intranasally and orally with mucosal adjuvants LT and LT(R192G) in BALB/c mice induce specific humoral and cellular Th1/Th2-like immune responses. *Vaccine* 22:1079.
29 Gao, W., Tamin, A., Soloff, A., D'Aiuto, L., Nwanegbo, E., Robbins, P. D., Bellini, W. J., Barratt-Boyes, S. and Gambotto, A. 2003. Effects of a SARS-associated coronavirus vaccine in monkeys. *Lancet* 362:1895.
30 Takamura, K., Matsumoto, Y. and Shimizu, Y. 2002. Field study of bovine coronavirus vaccine enriched with hemagglutinating antigen for winter dysentery in dairy cows. *Can. J. Vet. Res.* 66:278.
31 Pratelli, A., Tinelli, A., Decaro, N., Cirone, F., Elia, G., Roperto, S., Tempesta, M. and Buonavoglia, C. 2003. Efficacy of an inactivated canine coronavirus vaccine in pups. *New Microbiol.* 26:151.

JOURNAL OF CLINICAL MICROBIOLOGY, May 2004, p. 1956–1961
0095-1137/04/$08.00+0 DOI: 10.1128/JCM.42.5.1956–1961.2004

Vol. 42, No. 5

Development and Evaluation of a Novel Loop-Mediated Isothermal Amplification Method for Rapid Detection of Severe Acute Respiratory Syndrome Coronavirus

Hong Thi Cam Thai,[1] Mai Quynh Le,[2] Cuong Duc Vuong,[2] Manmohan Parida,[1] Harumi Minekawa,[3] Tsugunori Notomi,[3] Futoshi Hasebe,[1] and Kouichi Morita[1]*

Department of Virology, Institute of Tropical Medicine, Nagasaki University, Nagasaki 852-8523,[1] and Eiken Chemical Co. Ltd., Ohtawara, Tochigi 324-0036,[3] Japan, and Department of Virology, National Institute of Hygiene and Epidemiology, Hanoi, Vietnam[2]

Received 7 November 2003/Returned for modification 27 January 2003/Accepted 2 February 2004

The development and evaluation of a one-step single-tube accelerated real-time quantitative reverse transcription (RT) loop-mediated isothermal amplification (LAMP) assay is reported for rapid detection of the severe acute respiratory syndrome coronavirus (SARS-CoV) replicase gene. A total of 49 samples (15 throat washes, 13 throat swabs, and 21 combined throat and nasal swabs) collected from patients admitted to the Hanoi-French and Ninhbinh hospitals in Vietnam during the SARS epidemic were evaluated and compared to conventional RT-PCR. The RT-LAMP assay demonstrated 100-fold-greater sensitivity, with a detection limit of 0.01 PFU. The sensitivity and specificity of RT-LAMP assay for detecting viral RNA in clinical specimens with regard to RT-PCR were 100 and 87%, respectively. The specificity of the RT-LAMP assay was further validated by restriction analysis as well as nucleotide sequencing of the amplified product. The concentration of virus in most of the clinical samples was 0.1 PFU (0.1 to 10^2 PFU), as determined from the standard curve of SARS RT-LAMP and based on the time of positivity. The assay procedure is quite simple, wherein the amplification is carried out in a single tube under isothermal conditions at 63°C, and the result can be obtained in less than 1 h (as early as 11 min). Thus, the RT-LAMP assay reported here has the advantages of rapid amplification, simple operation, and easy detection and will be useful for rapid and reliable clinical diagnosis of SARS-CoV in developing countries.

Severe acute respiratory syndrome (SARS) is a recently emerged human disease associated with pneumonia. The fears of a SARS epidemic still loom throughout the world due to multicountry outbreak, rapid air travel, and spread into the wider community, especially among healthcare and laboratory workers. The outbreak is believed to have originated in November 2002 in the Guangdong province of China, with several hundred cases of severe atypical pneumonia (18, 21). Following the detection of similar cases in Hong Kong, Vietnam, and Canada, the World Health Organization (WHO) issued a global alert for the illness, designated SARS (7, 16, 20). The disease has since then spread rapidly around the world and caused 8,099 cases, with 774 deaths in 30 countries, spreading over five continents, with an economic loss estimated to be $50 billion to $100 billion worldwide (1, 4, 21).

The coordinated efforts of the WHO through international collaboration resolved the etiology of the SARS to be a novel coronavirus (CoV) with some unusual properties that had not previously been present in human populations (3, 6, 13). Unlike other human CoVs, SARS-CoV could be isolated in Vero cells. The genome of SARS-CoV is single-stranded, nonsegmented positive-sense RNA, which is 29,727 nucleotides in length with 11 open reading frames. The genome organization is similar to that of other CoVs with the characteristic gene order 5′-replicase (Rep)-spike-envelope-membrane-nucleocapsid-3′ and short untranslated regions at both termini (8, 18).

SARS is a type of viral pneumonia with an incubation period ranging from 2 to 7 days. The infection is usually characterized by fever, dry cough, dyspnea, headache, and hypoxemia (17). Death from progressive respiratory failure occurs in about 3% to nearly 10% of cases (14). The laboratory findings include lymphopenia and mildly elevated aminotransferase levels. Death may result from progressive respiratory failure due to alveolar damage in 3 to 6% cases (10, 16). The mechanism of transmission of the SARS virus is not yet fully established. The virus is believed to be spread by droplets produced by coughing and sneezing; however, other routes of transmission, such as fecal contamination, cannot be ruled out (2). Currently, there are no suitable antiviral drugs or an effective vaccine for SARS virus. Rapid laboratory confirmation of SARS-CoV infection is therefore important for managing patient care and for preventing nosocomial transmission. Thus, development of early, rapid, and reliable diagnostic assay systems for SARS-CoV is of top priority to strengthen the surveillance mechanisms for the prediction and prevention of large-scale epidemics in future.

The laboratory diagnosis of SARS-CoV is based on virus isolation, followed by electron microscopy studies to identify the virus on cell culture, which are technically very demanding. Serologically, the diagnosis is accomplished by looking for anti-

* Corresponding author. Mailing address: Department of Virology, Institute of Tropical Medicine, Nagasaki University, 1-12-4 Sakamoto, Nagasaki 852-8523, Japan. Phone: 81 95 849 7829. Fax: 81 95 849 7830. E-mail: moritak@net.nagasaki-u.ac.jp.

CoV antibodies by employing indirect fluorescent antibody testing and enzyme-linked immunosorbent assays. Although some patients have detectable CoV antibody within 14 days of illness onset, definitive interpretation of negative CoV antibody tests is possible only for specimens obtained >21 days after the onset of fever (11, 14). While serological testing is reliable as a retrospective diagnostic method, diagnosis of the infection in the early phase of the illness is important for patient care. To address the need for early and rapid identification of SARS-CoV, a reverse transcription (RT)-PCR-based assay was advocated by the WHO and is being routinely used for detecting virus-specific RNA (15, 22, 23). The existing PCR tests are reported to be very specific but lack the sensitivity and are time-consuming. The testing of more than one respiratory specimen is advocated for improved sensitivity of the existing PCR assays (23). More-sensitive and real-time-based assays are therefore needed to complement the existing PCR-based assay systems.

The present report describes the development and evaluation of a novel nucleic acid amplification method, termed loop-mediated isothermal amplification (LAMP), for the rapid detection of SARS-CoV in clinical specimens in Vietnam. The LAMP is a novel approach for nucleic acid amplification that amplifies DNA with high specificity, selectivity, and rapidity under isothermal conditions, thereby obviating the need for a thermal cycler (10, 12). The amplification efficiency of the LAMP method is extremely high because there is no time loss for thermal change due to its isothermal reaction. Since the amplification of DNA is directly correlated with the production of magnesium pyrophosphate, leading to turbidity, real-time monitoring of the LAMP reaction is possible by real-time measurement of turbidity in an inexpensive photometer (9). Therefore, the LAMP assay has emerged as a powerful tool to facilitate point-of-care genetic testing at the bedside. We report the development of a one-step single-tube accelerated real-time quantitative RT-LAMP assay for rapid detection of SARS-CoV. Data on the sensitivity and specificity of the method are reported, and applicability of the technology for clinical diagnosis of SARS is discussed.

MATERIALS AND METHODS

Clinical specimens. A total of 49 specimens comprising 15 throat washes, 13 throat swabs, and 21 combined throat and nasal swabs samples were collected from 45 patients with clinically suspected SARS admitted to the Hanoi-French and Ninhbinh hospitals during the SARS epidemic in Vietnam between 4 February and 7 March 2003. Of 45 patients, 10 had confirmed cases of SARS, as reported by the Centers for Disease Control and Prevention, and 35 patients who had cases that fulfilled the modified WHO definition (22) of SARS were grouped as having suspected and probable cases. All of the samples were collected on day 3 after the onset of illness.

Virus. The SARS-CoV isolated from the throat wash sample of one patient was used in this study for standardization of the RT-LAMP assay. Briefly, the monolayers of Vero E6 cells grown in a 15-cm^2 culture flask were adsorbed with 0.5 ml of the inoculum at 37°C for 2 h. Following adsorption, the inoculum was replenished with 10 ml of maintenance medium. Suitable mock-infected cell controls were also kept. The cells were then incubated at 37°C and observed daily for cytopathic effects. Upon observation of 80 to 100% cytopathic effect, the infected culture supernatant was clarified by light centrifugation at 700 × *g* for 10 min and stored in aliquots at −80°C until use. The quantification of virus infectivity was carried out in Vero E6 cells grown in 24-well tissue culture plates as per standard protocol (19). The resulting plaques were counted, and virus titer was determined.

Designing of primers. Oligonucleotide primers used for RT-LAMP amplification of SARS-CoV were designed from the open reading frame 1b Rep gene sequences obtained from GenBank (accession number NC-004718) after comparing the alignment of Rep gene sequences of CoVs from human, bovine, porcine, and avian origins. The sequences of the selected primers were conserved to other SARS-CoV Rep gene sequences. A set of six primers comprising two outer, two inner, and two loop primers that recognize eight distinct regions on the target sequence were designed by using the LAMP primer designing support software program (Net Laboratory, Kanagawa, Japan). The detailed sequences of primers used for amplification of SARS-CoV are shown in Fig. 1. The two outer primers are described as forward outer primer (F3) and backward outer primer (B3). The inner primers are described as forward inner primer (FIP) and backward inner primer (BIP). An additional two loop primers (loop F and loop B) were designed to accelerate the amplification reaction. FIP consists of a complementary sequence of F1 (Fig. 1) and a sense sequence of F2. BIP consists of a complementary sequence of B1 and a sense sequence of B2. The loop F and loop B primers are composed of the sequences that are complementary to the sequence between the F1 and F2 and B1 and B2 regions, respectively.

RNA extraction. The clinical specimens were suspended in viral transport medium. Following centrifugation at 6,500 × *g* for 1 min, the supernatant was collected. Viral RNA was extracted from 140 μl of the supernatant by using a QIAamp viral RNA mini kit (Qiagen, Hilden, Germany). The initial processing of specimens was performed under biosafety level 3 containment facilities. After lysis of the sample by the lysis buffer, the mixture was applied to a spin column as described by the manufacturer. The extracted RNA was eluted in a total volume of 60 μl of elution buffer and was stored at −70°C until further use.

RT-LAMP assay. The RT-LAMP reaction was carried out in a 25-μl (total) reaction mixture by using the Loopamp DNA amplification kit (Eiken Chemical Co. Ltd., Tochigi, Japan) containing 40 pmol (each) of the primers FIP and BIP, 5 pmol (each) of the outer primers F3 and B3, 20 pmol (each) of loop primers F and B, 1.4 mM concentrations of deoxynucleoside triphosphates, 0.8 M betaine, 0.1% Tween 20, 10 mM $(NH_4)_2SO_4$, 8 mM $MgSO_4$, 10 mM KCl, 20 mM Tris-HCl (pH 8.8), 8 U of *Bst* DNA polymerase (New England Biolabs), 0.625 U of avian myeloblastosis virus reverse transcriptase (Invitrogen), and the specified amounts of target RNA was incubated at 63°C for 60 min in a heating block, followed by heating at 80°C for 2 min to terminate the reaction. For the real-time monitoring of RT-LAMP assay, the reaction mixture was incubated at 63°C for 60 min in the Loopamp real-time turbidimeter (LA-200; Teramecs, Kyoto, Japan). Positive and negative controls were included in each run, and all precautions to prevent cross-contamination were observed.

Interpretation of RT-LAMP results. The real-time amplification by RT-LAMP assay was monitored through spectrophotometric analysis by recording the optical density at 400 nm every 6 s with the help of a Loopamp real-time turbidimeter (LA-200; Teramecs). The cutoff value for positivity by the real time RT-LAMP assay was determined by taking into account the real time to positivity (T_p, in minutes) at which the turbidity increases above the threshold value fixed at 0.1, which is two times more than the average turbidity value of the negative controls of several replicates. None of the positive samples tested multiple times showed positivity in terms of increased turbidity after 60 min. Therefore, a sample having T_p values of ≤60 min and turbidity above the threshold value of ≥0.1 was considered positive. In addition, 10-μl aliquots of RT-LAMP products were electrophoresed on a 3% NuSieve 3:1 agarose gel (BMA, Rockland, Maine) for electrophoresis in Tris-borate buffer, followed by staining with ethidium bromide and visualization on a UV transilluminator at 302 nm. The specificity of the RT-LAMP amplified product was further validated by restriction digestion with HpaI enzyme as well as by nucleotide sequencing of both digested and undigested products with two outer and two internal primers.

RT-PCR. To compare the sensitivity and specificity of the RT-LAMP assay, RT-PCR was performed with the primer sets designed by the WHO SARS network laboratory at the Bernhard-Nocht Institute in Hamburg, Germany with slight modifications. The sequences of these primers were 5′-ATGAATTACCA AGTCAATGGTTAC (BNIout-sense) and 5′-CATAACCAGTCGGTACAG CTAC (BNIout-antisense). Following cDNA synthesis with the reverse primer (BNIout-antisense) at 42°C for 30 min, the PCR amplification was carried out with the LA *Taq* PCR kit (TaKaRa Bio Inc., Shiga, Japan) by using 1 μl of cDNA and 50 pmol of each primer in a 50-μl total reaction volume according to the manufacturer's protocol. The thermal profile for RT-PCR was 94°C for 2 min, followed by 34 cycles of 94°C for 30 s, 54°C for 30 s, and 72°C for 30 s and a final extension cycle at 72°C for 10 min. The amplified products were then analyzed through a 3% NuSieve 3:1 agarose gel (BMA) by electrophoresis in Tris-borate buffer, and the target bands were visualized by staining with ethidium bromide.

Evaluation of RT-LAMP. The applicability of the RT-LAMP assay for detection of SARS-CoV RNA in clinical diagnosis was validated by evaluating the

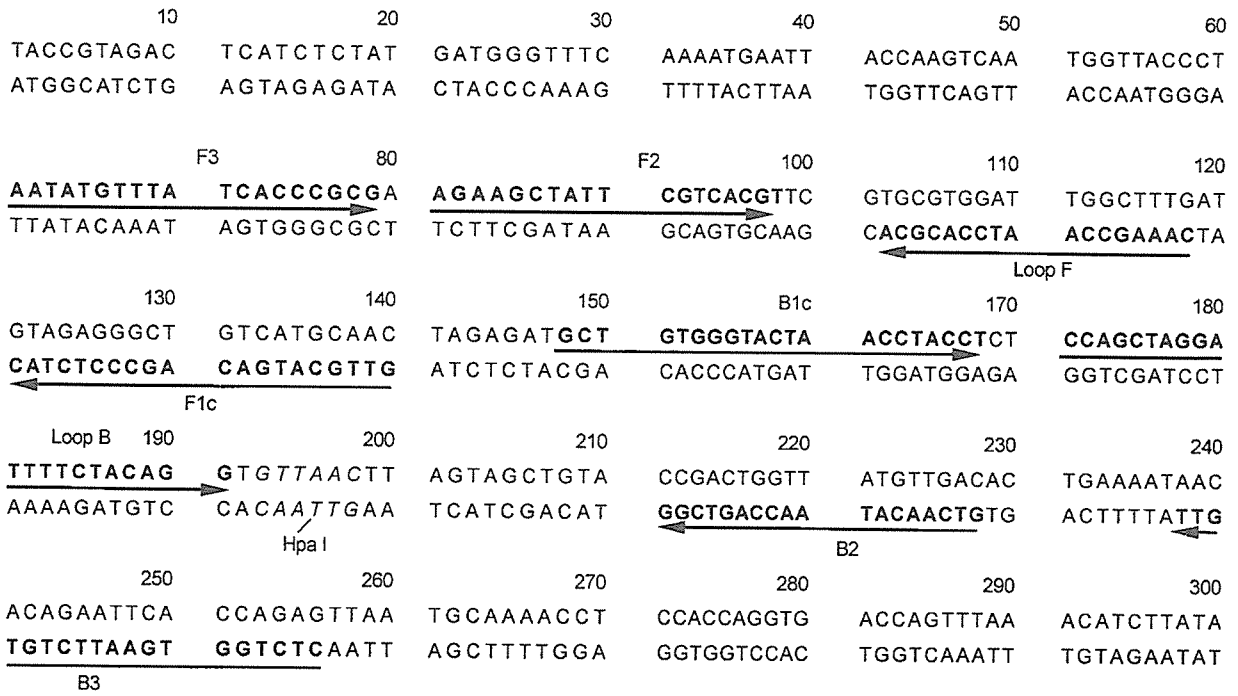

FIG. 1. Oligonucleotide primers used for RT-LAMP amplification of SARS-CoV (GenBank accession number NC-004718). The underlined letters indicate the sequences of primers.

assay system with the 49 samples (15 throat washes, 13 throat swabs, and 21 combined throat and nasal swabs) collected from patients admitted to hospitals as mentioned above. In addition, 10 throat wash samples collected from apparently healthy individuals were also included as negative controls. All 59 samples comprising 49 suspected SARS samples and 10 healthy samples were processed for RNA extraction by the QIAamp viral RNA mini kit and were screened by RT-LAMP and RT-PCR simultaneously for detection of viral RNA as described above.

RESULTS

The RT-LAMP assay was standardized with the SARS-CoV isolated from one of the patient throat wash samples. The identity of the isolated SARS-CoV was established by confirmation through RT-PCR with the specific primer sets described above. The RT-LAMP assay successfully amplified the 196-bp target sequence of the Rep gene of SARS-CoV at 63°C in 60 min, as observed by agarose gel electrophoresis. The amplification was observed as a ladder-like pattern on the gel due to the formation of a mixture of stem-loop DNAs with various stem lengths and cauliflower-like structures with multiple loops formed by annealing between alternately inverted repeats of the target sequence in the same strand (Fig. 2). The real-time kinetics of the RT-LAMP reaction revealed that the amplification signal with 10^4 PFU of virus could be detected as quickly as in 11 min, as indicated by the continuous increase in turbidity (Fig. 3), whereas the turbidity was fixed around 0.01, below the threshold value in the negative control which had no template.

Sensitivity and specificity of SARS RT-LAMP. To ascertain the detection limit of the RT-LAMP assay for the detection of SARS-CoV, serial 10-fold dilutions of virus that had been quantified by plaque assay were tested and compared with that of conventional RT-PCR. The detection limits for the RT-LAMP assay and RT-PCR were found to be 0.01 and 1 PFU, respectively (Fig. 4A and B, respectively). Thus, the comparative sensitivity of RT-LAMP and RT-PCR indicated that the RT-LAMP was 100-fold more sensitive than RT-PCR. The amplification by RT-LAMP showed a ladder-like pattern, whereas the RT-PCR showed a 195-bp amplicon (Fig. 4B). By

FIG. 2. Agarose gel electrophoresis and restriction analysis of RT-LAMP products of the Rep gene of SARS-CoV on a 3% agarose gel. Lane M, 100-bp DNA ladder (Sigma Genosys, Hokkaido, Japan); lane 1, RT-LAMP product of SARS-CoV digested with HpaI (135 bp); lane 2, RT-LAMP products of SARS-CoV; lane 3, RT-LAMP without target RNA.

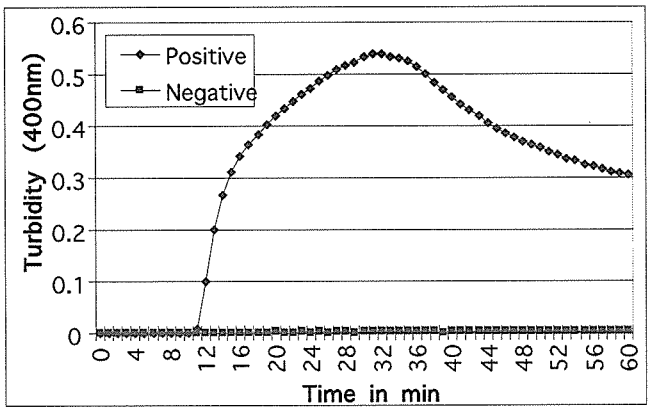

FIG. 3. Real-time kinetics of RT-LAMP amplification of SARS-CoV RNA, as monitored by real-time measurement of turbidity on a Loopamp real-time turbidimeter (LA-200; Teramecs).

real-time monitoring of the amplification of different concentrations of virus ranging from 10^4 to 0.01 PFU, a standard curve depicting the linear relationship between the concentration of virus (in PFU) to T_p was generated for SARS-CoV (Fig. 5A).

The specificity of the amplification was confirmed by digestion with restriction enzyme HpaI to ensure that the amplification product had the corresponding sequences of the selected target. The resultant digested product of 135 bp was in good agreement with the predicted size (Fig. 2). Further confirmation of the structures of the amplified products were also carried out by sequencing, wherein the sequences obtained perfectly matched with the expected nucleotide sequences (data not shown)

Evaluation of SARS RT-LAMP with clinical specimens. A total of 59 samples including 15 throat washes, 13 throat swabs, 21 combined throat and nasal swabs, and 10 healthy throat wash samples were screened by RT-LAMP and RT-PCR simultaneously. The RT-LAMP assay detected 13 positive samples and 46 negative samples; the RT-PCR assay detected 6 positive samples and 53 negative samples. A concordance of 88% (52 of 59) was observed between the two test systems. Of 59 samples, 6 were positive and 46 were negative by both tests. However, the RT-LAMP assay was able to detect SARS-CoV RNA in 7 additional specimens that were negative by RT-PCR. The sensitivity and specificity of the RT-LAMP assay with regard to RT-PCR were 100 and 87%, respectively. Of 15 throat wash samples, 67% (10 of 15) were positive by RT-LAMP compared to 27% positive by RT-PCR (Table 1). None of the throat swab samples were positive by any of the test systems. The concentration of the virus in different kinds of clinical samples was calculated from the standard curve based on their T_p values. Of 13 positive samples, 8 samples had a virus concentration of 0.1 PFU. The range of virus concentration among different kind of samples was 0.1 to 10^2 PFU (Fig. 5B). None of the healthy throat wash samples tested were positive, thereby indicating the specificity of the two assay systems.

DISCUSSION

SARS is a newly emerging life-threatening respiratory disease that has created international anxiety because of its nov-

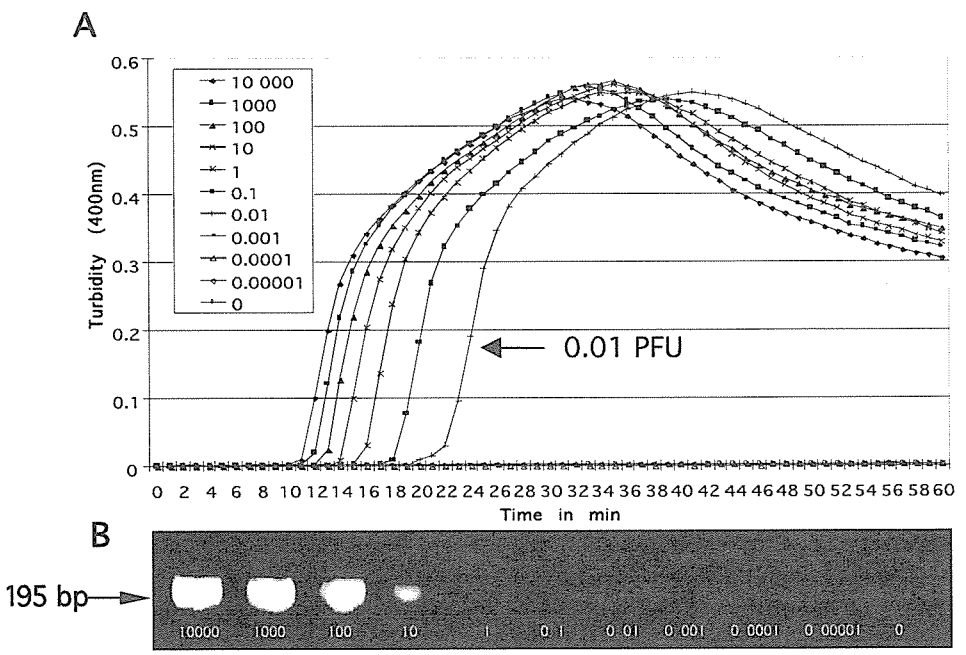

FIG. 4. Comparative sensitivity of RT-LAMP and RT-PCR for detection of SARS-CoV. The amplification by RT-LAMP (A) showed ladder-like pattern, whereas the RT-PCR (B) showed 195-bp amplification. (A) Sensitivity of SARS RT-LAMP assay as monitored by real-time measurement of turbidity (LA-200; Teramecs). Shown from left to right are the curves of decreasing concentrations of virus from 10,000 to 0.00001 PFU. The detection limit for the assay was 0.01 PFU. (B) Sensitivity of RT-PCR for the detection of SARS-CoV as observed by agarose gel analysis with a detection limit of 1 PFU.

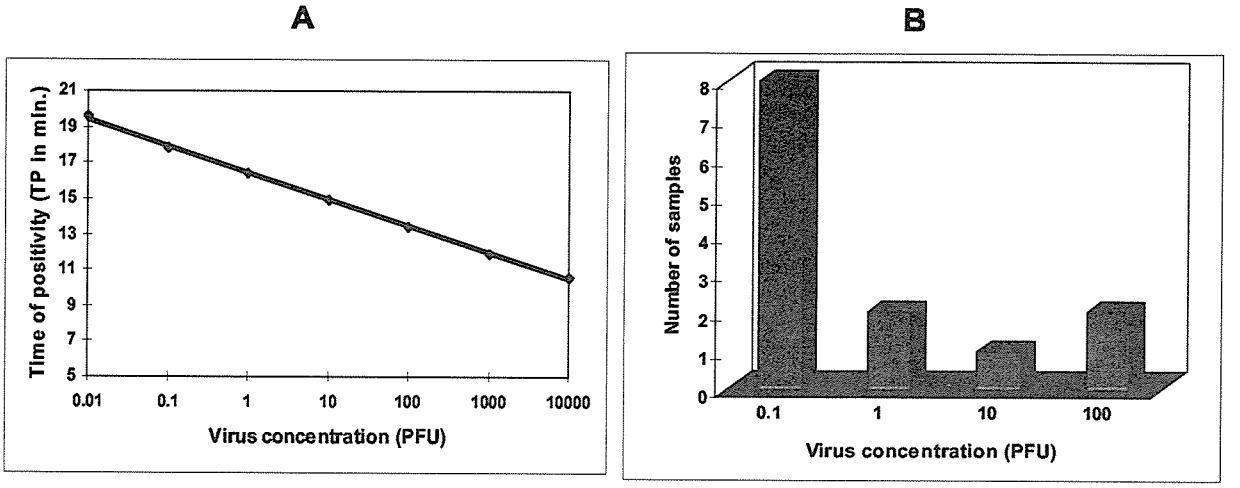

FIG. 5. Quantitative determination of virus concentration in clinical samples employing a standard curve of the SARS RT-LAMP assay. (A) Standard curve generated for SARS RT-LAMP assay by plotting T_p with regard to various concentrations of virus in PFU. (B) Determination of virus titer in clinical samples derived from the standard curve based on their T_p values.

elty, communicability, and rapid spread, leading to multicountry outbreak. The development of early, rapid, and reliable diagnostic assay systems are of high priority for early vigilance and timely implementation of control measures. The pace of SARS research has been astounding. The identification of the virus and subsequent availability of the SARS-CoV genome sequence is important from a public health perspective. This has led to the development of rapid and reliable PCR-based assays based on the novel sequence features helping in the discrimination of SARS from other circulating CoVs. SARS virus genome-based PCR assays formed an important part of a public health strategy to control the spread of this syndrome.

The prompt communication and exchange of information among the WHO collaborating laboratories facilitate the development of RT-PCR-based rapid diagnostic assays. This is now being routinely practiced all over the globe for rapid identification of SARS cases. In addition, quantitative PCR methods like a real-time PCR and *Taq*Man format assays to detect SARS-CoV in nasopharyngeal aspirate and stool samples have been developed (15). Despite the obtainable magnitude of amplification, these methods are time-consuming (e.g., RNA extraction, RT, and real-time PCR can be completed in 3 to 4 h) and more complicated and need a high-precision thermal cycler, and contamination of samples in laboratories may lead to false-positive results.

TABLE 1. Comparative evaluation of RT-LAMP assay and RT-PCR for detection of SARS-CoV RNA in clinical specimens

Type of specimen	No. of samples tested	% (no.) of positive samples for assay	
		RT-LAMP	RT-PCR
Throat wash	15	67 (10)	27 (4)
Throat swab	13	0	0
Throat and nasal swabs	21	14 (3)	10 (2)
Healthy throat wash	10	0	0
Total	59	22 (13)	10 (6)

On the contrary, the RT-LAMP assay reported here is advantageous due to its simple operation, rapid reaction, and easy detection. The RT-LAMP assay is a simple diagnosis tool in which the reaction is carried out in a single tube by mixing the buffer, primers, reverse transcriptase, and DNA polymerase and incubating the mixture at 63°C for 1 h in a regular laboratory water bath or heat block that provides a constant temperature of 63°C. The amplification can be performed in a shorter time than amplification by RT-PCR because there is no time loss due to thermal cycling. In addition, the specificity of the reaction is extremely high because it uses six primers recognizing eight distinct regions on the target DNA. The LAMP method was initially standardized for detection of hepatitis B virus DNA (12) and was recently applied for direct detection of the *Mycobacterium tuberculosis* complex, *Mycobacterium avium*, and *Mycobacterium intracellulare* in sputum samples (5). By using RNA as a template, the RT-LAMP assay has also been used for the detection of prostate-specific antigen mRNA in K562 cells (12).

We developed a one-step single-tube accelerated real-time quantitative RT-LAMP assay for the early and rapid diagnosis of SARS-CoV. The assay can detect SARS-CoV at an early stage of infection by using throat washes and combined throat and nasal swab specimens. The evaluation of the RT-LAMP assay for detection of viral RNA in clinical specimens has been validated with 59 samples, including 15 throat washes, 13 throat swabs, 21 combined throat and nasal swabs, and 10 healthy throat wash samples collected from the Hanoi-French and Ninhbinh hospitals during the SARS epidemic in Vietnam, and results were compared with those of conventional RT-PCR. Of 49 samples, 10 samples were confirmed to be SARS-CoV, as reported by the Centers for Disease Control and Prevention, by using virus isolation and/or nested RT-PCR methods, and 35 samples were grouped as probable or suspected cases based on the WHO case definition.

The data presented in this study suggested that the RT-LAMP assay is more sensitive than RT-PCR by picking up 7 additional cases that were negative by RT-PCR. It is pertinent

to note that all 7 of these samples were collected from confirmed cases of SARS. The RT-LAMP assay demonstrated exceptionally higher sensitivity than conventional RT-PCR. The RT-LAMP assay was found to be 100-fold more sensitive than RT-PCR, with a detection limit of 0.01 PFU in clinical samples. In addition, by using a real-time RT-LAMP assay, the quantitation of virus concentration in the clinical sample is possible, which will indicate the early stage of the virus infection as well as potential source transmitters.

Among the various types of clinical specimens overall, 22% of throat washes and 10% of combined throat and nasal swabs were positive by both RT-LAMP and RT-PCR assays employed in this study. None of the throat swab samples were positive by any of the test systems, indicating only that throat swab samples are not suitable for detection of SARS-CoV RNA. This is in agreement with those of previous studies (3, 6), wherein it was demonstrated that swab specimens yield less virus for detection by virus isolation. From a diagnostic point of view, it is important to note that nasal and throat swabs seem less suitable for diagnosis, since these materials contain considerably less viral RNA than throat washes, and the virus may escape detection if only these materials are tested. The throat wash samples were found to be the most suitable specimens for detection of SARS-CoV.

In conclusion, the one-step single-tube accelerated real-time quantitative RT-LAMP assay developed in this study is simple, rapid, and cost effective as well as highly sensitive and specific. This has potential usefulness for clinical diagnosis and surveillance of SARS virus in developing countries, as it does not require the use of sophisticated equipment or skilled personnel.

ACKNOWLEDGMENTS

The financial support for this study from the Ministry of Education, Culture, Sports, Science, and Technology in the form of a Monbusho scholarship [Grant-in-Aid for Scientific Research (B) 15406020] is thankfully acknowledged.

We are grateful to Hoang Thuy Long, Director, NIHE, Hanoi, Vietnam, for keen interest and support for this study. We are also thankful to Maria del Carmen Parquet for critical suggestions in the preparation of the manuscript and Guillermo Posadas for technical support in this study.

REFERENCES

1. **Centers for Disease Control and Prevention.** 2003. Update: outbreak of severe acute respiratory syndrome—worldwide, 2003. Morb. Mortal. Wkly. Rep. **52:**226–228.
2. **Donnelly, C. A., A. C. Ghani, G. M. Leung, A. J. Hedley, C. Fraser, S. Riley, L. J. Abu-Raddad, L. M. Ho, T. Q. Thach, P. Chau, K. Chan, T. H. Lam, L. Y. Tse, T. Tsang, S. H. Liu, J. H. B. Kong, E. M. C. Lau, N. M. Ferguson, and R. M. Anderson.** 2003. Epidemiological determinants of spread of causal agent of severe acute respiratory syndrome in Hong Kong. Lancet **361:**1761–1766.
3. **Drosten, C., S. Gunther, W. Preiser, S. van der Werf, H. R. Brodt, S. Becker, H. Rabenau, M. Panning, L. Kolesnikova, R. A. Fouchier, A. Berger, A. M. Burguiere, J. Cinatl, M. Eickmann, N. Escriou, K. Grywna, S. Kramme, J. C. Manuguerra, S. Muller, V. Rickerts, M. Sturmer, S. Vieth, H. D. Klenk, A. D. Osterhaus, H. Schmitz, and H. W. Doerr.** 2003. Identification of a novel coronavirus in patients with severe acute respiratory syndrome. N. Engl. J. Med. **348:**1967–1976.
4. **Epstein, R. P., E. Chivian, and K. Frith.** 2003. Emerging diseases threaten conservation. Environ. Health Perspect. **111:**A506–A507.
5. **Iwamoto, T., T. Sonobe, and K. Hayashi.** 2003. Loop-mediated isothermal amplification for direct detection of *Mycobacterium tuberculosis* complex, *M. avium*, and *M. intracellulare* in sputum samples. J. Clin. Microbiol. **41:**2616–2622.
6. **Ksiazek, T. G., D. Erdman, C. Goldsmith, et. al.** 2003. A novel corona virus associated with severe acute respiratory syndrome. N. Engl. J. Med. **348:**1953–1966.
7. **Lee, N., D. Hui, A. Wu, P. Chan, P. Cameron, G. M. Joynt, A. Ahuja, M. Y. Yung, C. B. Leung, K. F. To, S. F. Lui, C. C. Szeto, S. Chung, and J. J. Sung.** 2003. A major outbreak of severe acute respiratory syndrome in Hong Kong. N. Engl. J. Med. **348:**1986–1994.
8. **Marra, M. A., S. J. Jones, C. R. Astell, R. A. Holt, A. Brooks-Wilson, Y. S. Butterfield, J. Khattra, J. K. Asano, S. A. Barber, S. Y. Chan, A. Cloutier, S. M. Coughlin, D. Freeman, N. Girn, O. L. Griffith, S. R. Leach, M. Mayo, H. McDonald, S. B. Montgomery, P. K. Pandoh, A. S. Petrescu, A. G. Robertson, J. E. Schein, A. Siddiqui, D. E. Smailus, J. M. Stott, G. S. Yang, F. Plummer, A. Andonov, H. Artsob, N. Bastien, K. Bernard, T. F. Booth, D. Bowness, M. Drebot, L. Fernando, R. Flick, M. Garbutt, M. Gray, A. Grolla, S. Jones, H. Feldmann, A. Meyers, A. Kabani, Y. Li, S. Normand, U. Stroher, G. A. Tipples, S. Tyler, R. Vogrig, D. Ward, B. Watson, R. C. Brunham, M. Krajden, M. Petric, D. M. Skowronski, C. Upton, and R. L. Roper.** 2003. The genome sequence of the SARS-associated coronavirus. Science **300:**1399–1404.
9. **Mori, Y., K. Nagamine, N. Tomita, and T. Notomi.** 2001. Detection of loop mediated isothermal amplification reaction by turbidity derived from magnesium pyrophosphate formation. Biochem. Biophys. Res. Commun. **289:**150–154.
10. **Nagamine, K., T. Hase, and T. Notomi.** 2002. Accelerated reaction by loop mediated isothermal amplification using loop primers. Mol. Cell. Probes **16:**223–229.
11. **Nie, Q. H., X. D. Luo, and W. L. Hui.** 2003. Advances in clinical diagnosis and treatment of severe acute respiratory syndrome. World J. Gastroenterol. **9:**1139–1143.
12. **Notomi, T., H. Okayama, H. Masubuchi, T. Yonekawa, K. Watanabe, N. Amino, and T. Hase.** 2000. Loop-mediated isothermal amplification of DNA. Nucleic Acids Res. **28:**E63.
13. **Peiris, J. S. M., S. Lai, L. L. M. Poon, Y. Guan, L. Yam, W. Lim, J. Nicholls, W. Yee, W. Yan, M. Cheung, V. Chen, K. H. Chan, D. Tsang, R. Yung, T. Ng, and K. Y. Yuen.** 2003. Coronavirus as a possible cause of severe acute respiratory syndrome. Lancet **361:**1319–1325.
14. **Peiris, J. S. M., C. M. Chu, V. C. Cheng, K. S. Chan, I. F. Hung, L. L. Poon, K. I. Law, B. S. Tang, T. Y. Hon, C. S. Chan, K. H. Chan, J. S. Ng, B. J. Zheng, W. L. Ng, R. W. Lai, Y. Guan, K. Y. Yuen, and HKU/UCH SARS Study Group.** 2003. Clinical progression and viral load in a community outbreak of coronavirus-associated SARS pneumonia: a prospective study. Lancet **361:**1767–1772.
15. **Poon, L. L., O. K. Wong, K. H. Chan, W. Luk, K. Y. Yuen, J. S. Peiris, and Y. Guan.** 2003. Rapid diagnosis of a coronavirus associated with severe acute respiratory syndrome (SARS). Clin. Chem. **49:**953–955.
16. **Poutanen, S. M., S. Finkelstein, R. Tellier, M. Ayers, D. Skowronski, A. S. Slutsky, and M. Petric.** 2003. Identification of severe acute respiratory syndrome in Canada. N. Engl. J. Med. **348:**1995–2005.
17. **Rainer, T. H., P. A. Cameron, D. Smit, K. L. Ong, A. N. Hung, D. C. Nin, A. T. Ahuja, L. C. Si, and J. J. Sung.** 2003. Evaluation of W. H. O. criteria for identifying patients with severe acute respiratory syndrome out of hospital: prospective observational study. BMJ **326:**1354–1358.
18. **Rota, P. A., M. S. Oberste, S. S. Monroe, W. A. Nix, R. Campagnoli, J. P. Icenogle, S. Penaranda, B. Bankamp, K. Maher, M. H. Chen, S. Tong, A. Tamin, L. Lowe, M. Frace, J. L. DeRisi, Q. Chen, D. Wang, D. D. Erdman, T. C. Peret, C. Burns, T. G. Ksiazek, P. E. Rollin, A. Sanchez, S. Liffick, B. Holloway, J. Limor, K. McCaustland, M. Olsen-Rasmussen, R. Fouchier, S. Gunther, A. D. Osterhaus, C. Drosten, M. A. Pallansch, L. J. Anderson, W. J. Bellini.** 2003. Characterization of a novel coronavirus associated with severe acute respiratory syndrome. Science **300:**1394–1399.
19. **Schmidt, N. J.** 1979. Cell culture techniques for diagnostic virology, p. 115–139. *In* E. H. Lennette and N. J. Schmidt (ed.), Diagnostic procedures for viral, rickettsial, and chlamydial infections, 5th ed. American Public Health Association, New York, N.Y.
20. **Tsang, K. W., P. L. Ho, G. C. Ooi, W. K. Yee, T. Wang, M. Chan-Yeung, W. K. Lam, W. H. Seto, L. Y. Yam, T. M. Cheung, P. C. Wong, B. Lam, M. S. Ip, J. Chan, K. Y. Yuen, and K. N. Lai.** 2003. A cluster of cases of severe acute respiratory syndrome in Hong Kong. N. Engl. J. Med. **348:**1977–1985.
21. **World Health Organization.** 2003. Severe acute respiratory syndrome (SARS). Wkly. Epidemiol. Rec. **78:**86–87.
22. **World Health Organization Multicentre Collaborative Network for Severe Acute Respiratory Syndrome Diagnosis.** 2003. A multicentre collaboration to investigate the cause of severe acute respiratory syndrome. Lancet **361:**1730–1733.
23. **Yam, W. C., K. H. Chan, L. L. M. Poon, Y. Guan, K. Y. Yuen, W. H. Seto, and J. S. M. Peiris.** 2003. Evaluation of reverse transcription-PCR assays for rapid diagnosis of severe acute respiratory syndrome associated with a novel coronavirus. J. Clin. Microbiol. **141:**4521–4524.

nature medicine

Pegylated interferon-α protects type 1 pneumocytes against SARS coronavirus infection in macaques

Bart L Haagmans[1,6], Thijs Kuiken[1,6], Byron E Martina[1], Ron A M Fouchier[1], Guus F Rimmelzwaan[1], Geert van Amerongen[1], Debby van Riel[2], Ton de Jong[3], Shigeyuki Itamura[4], Kwok-Hung Chan[5], Masato Tashiro[4] & Albert D M E Osterhaus[1]

The primary cause of severe acute respiratory syndrome (SARS) is a newly discovered coronavirus[1–7]. Replication of this SARS coronavirus (SCV) occurs mainly in the lower respiratory tract, and causes diffuse alveolar damage[2,7,8]. Lack of understanding of the pathogenesis of SARS has prevented the rational development of a therapy against this disease. Here we show extensive SCV antigen expression in type 1 pneumocytes of experimentally infected cynomolgus macaques (*Macaca fascicularis*) at 4 d postinfection (d.p.i.), indicating that this cell type is the primary target for SCV infection early in the disease, and explaining the subsequent pulmonary damage. We also show that prophylactic treatment of SCV-infected macaques with the antiviral agent pegylated interferon-α (IFN-α) significantly reduces viral replication and excretion, viral antigen expression by type 1 pneumocytes and pulmonary damage, compared with untreated macaques. Postexposure treatment with pegylated IFN-α yielded intermediate results. We therefore suggest that pegylated IFN-α protects type 1 pneumocytes from SCV infection, and should be considered a candidate drug for SARS therapy

SARS has recently emerged in the human population as a potentially fatal respiratory disease. Severely affected patients develop acute respiratory distress syndrome[7–10], which corresponds with diffuse alveolar damage (DAD) at autopsy[2,11]. A newly discovered coronavirus, SCV, has been identified as the primary cause of SARS[1,2,5–7]. SARS patients have been treated empirically with a combination of ribavirin, oseltamivir, antibiotics and corticosteroids[7–9]. However, neither case-control studies nor animal models have been used to determine the efficacy of these drugs. The choice and evaluation of potential drugs is also hampered by poor understanding of the pathogenesis of SARS.

We previously hypothesized that SCV infects type 1 pneumocytes, based on the character of the pulmonary lesions in experimentally infected macaques and the known tropism of other respiratory coronaviruses for type 1 pneumocytes[2]. We found extensive type 2 pneumocyte hyperplasia in the lungs of SCV-infected macaques at 6 d.p.i., suggesting that there had been loss of type 1 pneumocytes at an earlier stage of infection[2,12]. To determine whether type 1 pneumocytes are infected by SCV at an earlier stage of infection, we conducted pathological and immunohistochemical examinations of the lungs of four SCV-infected macaques (control group) at 4 d.p.i.. The lungs had multifocal, acute DAD, which was characterized by flooding of alveoli with protein-rich edema fluid mixed with neutrophils and rare syncytia, extensive loss of alveolar and bronchiolar epithelium, and occasional type 2 pneumocyte hyperplasia (Fig. 1a; for comparison, normal alveolar morphology is seen in Fig. 1b). Immunohistochemistry revealed extensive SCV antigen expression by squamous cells lining the alveolar walls (Fig. 1c,d; compare with Fig. 1e). These cells were identified as type 1 pneumocytes by their location, morphology and expression of keratin in serial sections. Transmission electron microscopy of alveolar cells revealed coronavirus-like particles measuring about 70 nm in diameter with typical internal nucleocapsid-like structure (Fig. 1f,g). These cells were identified as type 1 pneumocytes because they lined the alveolar lumen, were closely apposed to the basement membrane, were squamous, contained abundant pinocytotic vesicles, and—in contrast to type 2 pneumocytes—had neither lamellar bodies nor microvilli[13]. As found previously in experimentally infected macaques at 6 d.p.i., less extensive SCV antigen expression also was detected in hyperplastic type 2 pneumocytes within inflammatory foci[2] (Fig. 1h). Together, these histopathologic and immunohistochemical findings show that type 1 pneumocytes are the main target of SCV in early infection, and are associated with DAD.

An effective antiviral agent for the treatment of SCV infection is needed because decreasing viral replication in the first phase of SARS may reduce the severity of subsequent pathological damage, as has been found in another model of viral-induced DAD[14,15]. IFN-α may inhibit replication of animal and human coronaviruses[16–18]. As a candidate drug, we tested the efficacy of pegylated recombinant IFN-α2b, a registered drug for the treatment of chronic hepatitis C[19]. We chose this drug because it is registered and therefore directly available, because human recombinant IFNs inhibit SCV replication *in vitro*[20], and because pegylation optimizes the

[1]Department of Virology, [2]Department of Immunology and [3]Department of Pathology, Erasmus Medical Centre, PO Box 1738, 3000 DR, Rotterdam, Netherlands. [4]Department of Viral Diseases & Vaccine Control, National Institute of Infectious Diseases, Tokyo 208-0011, Japan. [5]Department of Microbiology and Pathology, Queen Mary Hospital, University of Hong Kong SAR, China. [6]These authors contributed equally to this work. Correspondence should be addressed to A.D.M.E.O. (a.osterhaus@erasmusmc.nl).

Published online 22 February 2004; doi:10.1038/nm1001

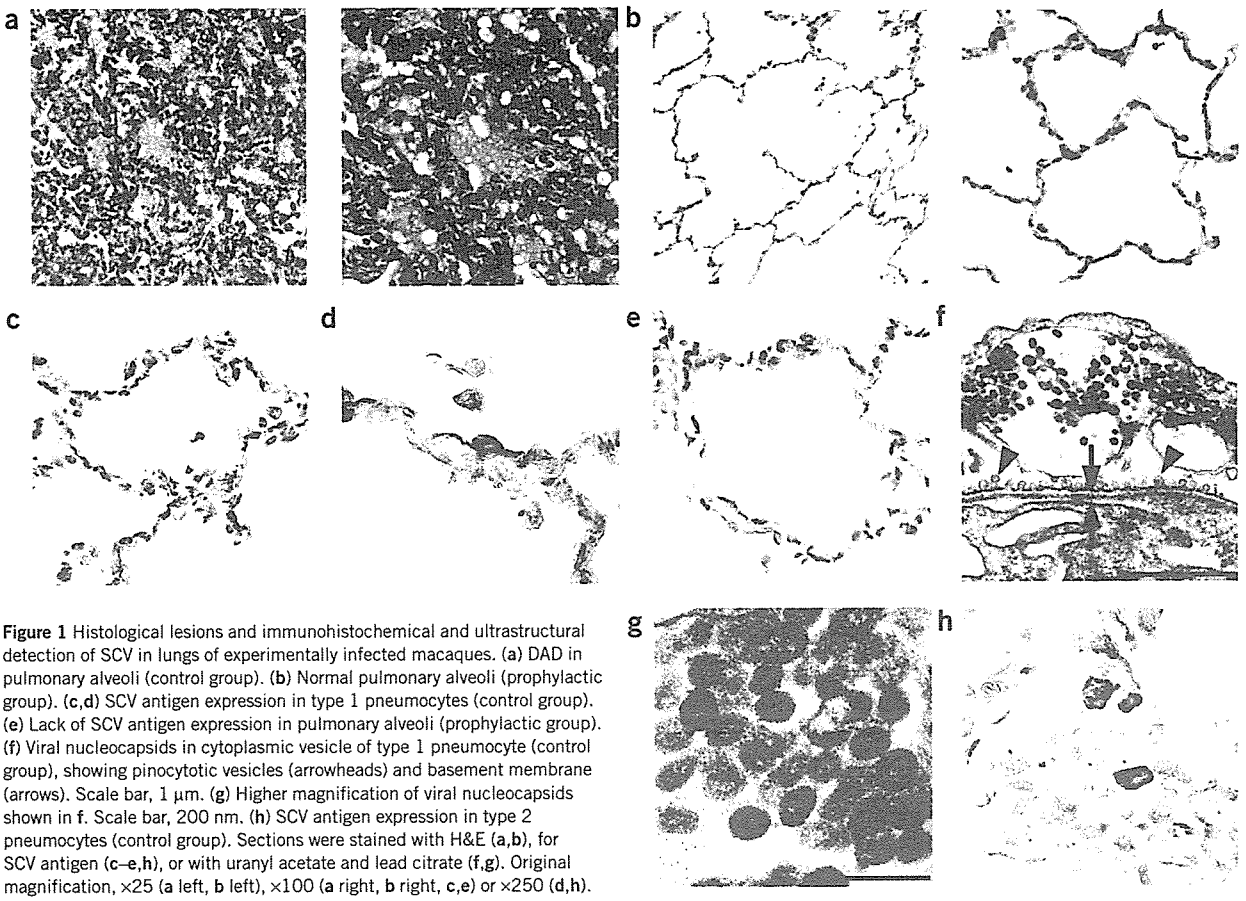

Figure 1 Histological lesions and immunohistochemical and ultrastructural detection of SCV in lungs of experimentally infected macaques. (**a**) DAD in pulmonary alveoli (control group). (**b**) Normal pulmonary alveoli (prophylactic group). (**c**,**d**) SCV antigen expression in type 1 pneumocytes (control group). (**e**) Lack of SCV antigen expression in pulmonary alveoli (prophylactic group). (**f**) Viral nucleocapsids in cytoplasmic vesicle of type 1 pneumocyte (control group), showing pinocytotic vesicles (arrowheads) and basement membrane (arrows). Scale bar, 1 μm. (**g**) Higher magnification of viral nucleocapsids shown in **f**. Scale bar, 200 nm. (**h**) SCV antigen expression in type 2 pneumocytes (control group). Sections were stained with H&E (**a**,**b**), for SCV antigen (**c**–**e**,**h**), or with uranyl acetate and lead citrate (**f**,**g**). Original magnification, ×25 (**a** left, **b** left), ×100 (**a** right, **b** right, **c**,**e**) or ×250 (**d**,**h**).

pharmacokinetic properties of IFN[21]. We first tested the effect of pegylated IFN-α on SCV-infected Vero cells, and observed a dose-dependent antiviral effect (Fig. 2a). We then determined the plasma levels of pegylated IFN-α after intramuscular injection into a group of six macaques (prophylactic group). High plasma levels were attained 1 d after injection (Fig. 2b), similar to peak levels found in patients after subcutaneous injection with 3-μg/kg pegylated IFN-α[21]. Because IFN-α is known to activate macrophages[22], we measured plasma levels of neopterin after pegylated IFN-α treatment, as a measure of macrophage activation. Neopterin levels were increased in all animals (Fig. 2c), confirming the biological availability of pegylated IFN-α in the treated macaques.

To evaluate the prophylactic use of pegylated IFN-α, we experimentally infected the macaques in the prophylactic group with SCV 3 d after the start of pegylated IFN-α treatment, and compared virological and pathological parameters with a control group of four macaques treated with PBS. We limited our investigation to pharyngeal swabs and the lung because an earlier study did not provide evidence of extensive viral replication in other organs[2]. We found that all parameters were significantly ($P < 0.05$) reduced in the prophylactic group compared with the control group. Virus excretion from the pharynx was abrogated (Fig. 3), and the virus titer in the lungs at 4 d.p.i. was significantly ($P < 0.01$) reduced (Fig. 4a). Immunohistochemistry showed that expression of SCV antigen in type 1 pneumocytes was reduced by 90% (Figs. 1e and 4b). By pathology, the extent and severity of DAD was reduced by 80% (Figs. 1b and 4c). These data indicate that prophylactic use of pegylated IFN-α substantially, although not completely, protects type 1 pneumocytes of experimentally infected macaques from SCV infection, with abrogation of virus excretion and reduced severity of pulmonary lesions.

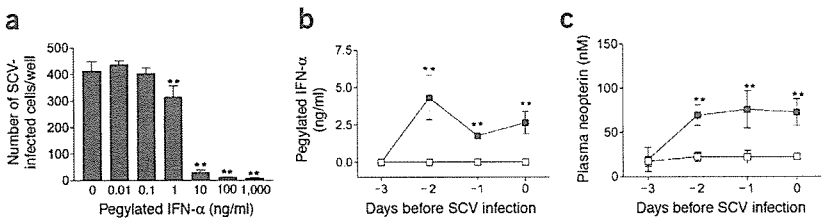

Figure 2 Antiviral activity of pegylated IFN-α against SCV *in vitro* and its biological activity in macaques. (**a**) Effect of pegylated IFN-α against SCV infection *in vitro*. Similar results were obtained in three separate experiments. (**b**) Pharmacokinetic analysis of pegylated IFN-α (**b**) and induction of neopterin (**c**) in macaques treated with PBS (□, control group; $n = 4$) or pegylated IFN-α (■, prophylactic group; $n = 4$) on days –3 and –1. Data are expressed as mean ± s.d. **, $P < 0.01$ compared with control.